
High-definition Brain Network (HDBN) Delineation of CDKL5 Deficiency Disorder (CDD) in Genetically Engineered Mice

[Dalton West](#) , [Noah William Coulson](#) , [Devin Raine Everaldo Cortes](#) , Kristina Elsa Schwab ,
Thomas Becker-Szurszewski , Sean Hartwick , Margaret Caroline Stapleton , [Gabriella Marie Saladino](#) ,
[Cecilia Wen-Ya Lo](#) , [Christina M Patterson](#) , [Subramanian Subramanian](#) , Deepa Soundara Rajan ,
[Yijen Lin Wu](#) *

Posted Date: 9 February 2026

doi: 10.20944/preprints202602.0539.v1

Keywords: CDKL5; CDD; MRI; neurodevelopment; brain network; diffusion tensor imaging



Preprints.org is a free multidisciplinary platform providing preprint service that is dedicated to making early versions of research outputs permanently available and citable. Preprints posted at Preprints.org appear in Web of Science, Crossref, Google Scholar, Scilit, Europe PMC.

Copyright: This open access article is published under a [Creative Commons CC BY 4.0 license](#), which permit the free download, distribution, and reuse, provided that the author and preprint are cited in any reuse.

Disclaimer/Publisher's Note: The statements, opinions, and data contained in all publications are solely those of the individual author(s) and contributor(s) and not of MDPI and/or the editor(s). MDPI and/or the editor(s) disclaim responsibility for any injury to people or property resulting from any ideas, methods, instructions, or products referred to in the content.

Article

High-definition Brain Network (HDBN) Delineation of CDKL5 Deficiency Disorder (CDD) in Genetically Engineered Mice

Dalton West ^{1,†}, Noah William Coulson ^{1,†}, Devin Raine Everaldo Cortes ^{1,2,3}, Kristina Elsa Schwab ^{1,3}, Thomas Becker-Szurszewski ^{1,3}, Sean Hartwick ^{1,3}, Margaret Caroline Stapleton ¹, Gabriella Marie Saladino ¹, Cecilia Wen-Ya Lo ¹, Christina M. Patterson ^{1,5}, Subramanian Subramanian ^{4,5}, Deepa Soundara Rajan ^{1,5} and Yijen Lin Wu ^{1,2,3,*}

¹ Department of Pediatrics, School of Medicine, University of Pittsburgh, Pittsburgh, PA, USA

² Department of Bioengineering, Swanson School of Engineering, University of Pittsburgh, Pittsburgh, PA, USA

³ Animal Imaging Core, Rangos Research Center at UPMC Children's Hospital of Pittsburgh, Pittsburgh, PA, USA

⁴ Department of Radiology, School of Medicine, University of Pittsburgh, Pittsburgh, PA, USA

⁵ UPMC Children's Hospital of Pittsburgh, Pittsburgh, PA, USA

* Correspondence: yijenwu@pitt.edu

† Equal contribution.

Abstract

Cyclin-Dependent Kinase-Like 5 (CDKL5) Deficient Disorder (CDD) is a rare X-linked developmental and epileptic encephalopathy characterized by early-onset refractory epilepsy, severe neurodevelopmental impairment, and lifelong disability. Although more than thirty anti-seizure medications are available, most CDD patients remain pharmaco-resistant. Gene-based therapies are emerging, but therapeutic development is hindered by marked clinical heterogeneity, small patient populations, and the lack of robust, translatable brain-based biomarkers for clinical trials. Genetically engineered *Cdkl5* mouse models recapitulate many cognitive, behavioral, and molecular features of CDD, yet their utility is limited by the absence of overt seizures, precluding seizure-based outcome measures. Here, we establish high-definition brain network (HDBN) biomarkers using advanced diffusion MRI tractography combined with graph-theoretical analysis to quantify whole-brain network organization in *Cdkl5* knockout mice. Diffusion MRI enables non-invasive mapping of axonal connectivity by leveraging anisotropic water diffusion, while high-angular-resolution acquisition overcomes key limitations of conventional diffusion tensor imaging in regions with complex fiber architecture. We demonstrate that *Cdkl5* knockout mice exhibit reproducible and region-specific disruptions in brain network organization, prominently affecting the somatosensory and somatomotor cortex, hippocampus, hypothalamus, amygdala, and superior colliculus—regions implicated in cognition, learning and memory, homeostasis, anxiety, and visual-motor function. In contrast, networks within the entorhinal cortex remain largely preserved. These findings identify HDBN metrics as sensitive, non-invasive biomarkers that capture clinically relevant circuit-level abnormalities in CDD. Because diffusion MRI-based network analyses are directly translatable across species, HDBN biomarkers provide a unified framework for therapeutic evaluation in mouse models, large animals, and human clinical trials, enabling longitudinal monitoring of disease progression and treatment response.

Keywords: CDKL5; CDD; MRI; neurodevelopment; brain network; diffusion tensor imaging

1. Introduction

Cyclin-Dependent Kinase-Like 5 (CDKL5) Deficient Disorder (CDD)[1–4], affecting ~2.36 per 100,000 live births, is an X-linked (*Xp22.13*, OMIM #300203)[5–9] developmental and epileptic encephalopathy (DEE2, OMIM #300672) characterized by early-onset refractory epilepsy, hypotonia, cortical visual impairments, global developmental delay, sensorimotor, speech abnormalities, and intellectual disabilities[1–4,10–12]. CDD and Rett syndrome show substantial clinical and biological overlaps, which is why CDD was historically considered an early-onset variant of Rett syndrome [10,13,14]. Caused by different genetic mutations (CDD- *CDKL5*, Rett – *MECP2*), they are now recognized as distinct but related DEE within the Rett spectrum [10,15]. The *CDKL5* gene encodes a serine/threonine protein kinase active in the brain and is essential for both neurodevelopment and normal neuronal function[10,16]. *CDKL5* protein plays a major role in the growth and migration of neurons[10], as well as synaptic signaling and cellular division[10]. Although more than thirty anti-seizure medications (ASMs)[17] are now available in the U.S., most CDD patients are not responding to current ASMs[3,18], continuing to have frequent seizures. No effective cure is available[19]. Even Ztalmy (ganaxolone)[20]—an ASM for CDD-associated seizures that was approved by the Food and Drug Administration (FDA) in 2022—does not eliminate the high disease burden for health care systems[21,22] and caregivers[23–25]. Even if seizures can sometimes be controlled, CDD patients still suffer neurodevelopmental deficits (NDD), greatly impacting their quality of life. There is an unmet clinical need for new CDD intervention. Several gene therapy[26–31] efforts are underway to treat CDD. However, CDD patients present highly heterogeneous[10,11,32] clinical manifestations and varied temporal progression courses. Compounded with low prevalence and small patient populations[33], these make clinical trials for therapeutic development for CDD very challenging. It lacks robust brain-based biomarkers for CDD clinical trials.

Genetically engineered mouse (GEM) models are indispensable for modeling human diseases for mechanistical understanding and therapeutic development. *Cdkl5* knockout (KO)[34] and knock-in (KI)[35] mice have existed for several years. *Cdkl5* mice recapitulated some cognitive and behavioral deficits[36,37] similar to those in CDD patients, as well as molecular and pathological features[38,39]. However, their pre-clinical utility for developing new therapeutics has been hampered by a key deficit - *Cdkl5* KO or KI mice do not exhibit overt seizures as CDD patients, thus one is unable to use seizures for therapeutic screening. Although some aged *Cdkl5* mice can display heterogeneous epileptic spasm[40] and age-related cognitive and motor declines[41,42], it is inappropriate to use aging phenotypes for neurodevelopmental investigations, because aged wild-type (WT) mice can also display epileptic spasm[43]. There is a major gap of a robust, brain-based biomarker for utilizing *Cdkl5* mice for therapeutic development. Although large animal models of CDD which may exhibit seizures are being developed, there are no inbred strains for pigs or non-human primates, resulting in heterogeneous and variable manifestations of CDD symptoms similar to humans. The same challenge of human clinical trials remains in the large animal models of CDD.

The goal of this study is to establish clinically relevant brain-based biomarkers that will enable therapeutic testing of not only *Cdkl5* KO mice, but of large animals and human clinical trials as well. Similar to human CDD patients, *Cdkl5* KO mice exhibit impairments in spatial learning and memory and anxiety- and fear-related behaviors[36]. Cognitive functions are carried by unique organizations of the brain network, the “information highways,” to process signals and information in the brain. We hypothesize that *Cdkl5* KO mice and CDD patients have altered brain network organization, resulting in cognitive deficits. This notion is consistent with the observation that loss of glutamatergic neurons in the hippocampus of *Cdkl5* KO mice disrupted the hippocampal micro-circuitry leading to impaired spatial learning and memory[39].

Diffusion MRI tractography is a non-invasive way to map neuronal connections in the entire brain. Diffusion MRI[44–52] leverages anisotropic water diffusion properties in the biological tissue to generate MRI contrast[53,54], providing a non-invasive way to map white matter connections. In neuronal fibers, water molecules can readily diffuse along neuronal fiber orientation, but are very limited perpendicular to the neuronal fiber orientation due to diffusion barriers of cell membranes

and myeline sheath[55–58], allowing non-invasive mapping of neuronal track orientations and connections in the brain. Diffusion tractography models water diffusion patterns in neuronal axons as a Gaussian distribution, and the determination of axonal direction by the principal direction of the tensor[44,45]. Based on this principal direction, the trajectories of the axonal connections can be tracked by diffusion fiber tractography, a computational approach which reveals the axonal orientations and connections between brain areas[59,60].

Diffusion tensor imaging (DTI)[44,45] is by far the most popular diffusion MRI model used. However, its major limitations have been well documented[61–63], as it is known to be limited to a coherent fiber population in large voxels and cannot model structures with complex fiber orientations. To overcome limitations of conventional DTI, this project leverages high-definition diffusion MRI with high angular resolutions in conjunction with brain topological analysis with graph theory to establish robust high-definition brain network (HDBN) analysis in *Cdkl5* KO mice. We have successfully established HDBN characteristics in *Cdkl5* KO mice corresponding to their cognitive and behavioral deficits. As diffusion MRI and HDBN analysis can be non-invasively conducted in live humans and large animals, HDBN-based biomarkers can be readily applicable for large animal studies and human translation for clinical trials. It is conceivable to compare HDBN-based biomarkers before and after gene therapy, or to monitor longitudinal CDD progression and regression with pharmacological interventions.

Our data demonstrate that HDBN can sensitively delineate brain network architecture in *Cdkl5* KO mice, to distinguish them from WT mice. *Cdkl5* KO mice displayed markedly altered neuronal network organization in the somatosensory and somatomotor cortices, hippocampus, hypothalamus, amygdala, and superior colliculus. These are the brain regions involved in cognition, learning and memory, homeostasis, anxiety and fear-condition, and visual/motor functions, respectively. This is consistent with the clinical presentations of CDD patients with cognitive, learning and memory deficits, anxiety, and cortical visual impairments. On the other hand, the entorhinal cortex, part of the olfactory circuitry, appears to be normal.

HDBN can sensitively detect brain network in CDD mouse models correlated with clinical presentations of CDD patients. As HDBN characteristics are qualitative and reproducible, it can potentially be a brain-based biomarker for therapeutic development in large animal models and clinical trials.

2. Materials and Methods

2.1. Animals

All animals received humane care in compliance with the NIH Office of Laboratory Animal Welfare (OLAW) guidelines. Animal protocols were approved by the University of Pittsburgh Institutional Animal Care and Use Committee (IACUC Protocol # 25066689, valid until June 4th, 2028). Mice were provided with *ad libitum* water and chow. *Cdkl5*[34] breeding pairs were obtained from the Jackson Laboratory (B6.129(FVB)-*Cdkl5*^{tm1.1joez}/J, Jax Strain #: 021967) as well as BL6/J (C57BL/6J, Jax Strain # 000664). Hemizygous *Cdkl5* males (Y/−, n=12) and male BL6/J (n=8) were included in the study. All animals were weaned on post-natal day p28. Male littermates were housed with 2-4 littermates per cage on a 12:12 hour dark/light schedule. Brains were harvested for diffusion MRI at 3.5-5 months. Animals were euthanized with 5% isoflurane followed by cervical dislocation. The heart was exposed with a chest incision through the ribs. The brain was then perfused with 7 mL of 4% paraformaldehyde (PFA) via cardiac perfusion. The brain was then harvested and placed in 4% PFA for at least two days at 4°C. The brain was then placed in phosphate buffered saline (PBS) at 4°C for two days for re-hydration before imaging.

2.2. High-Resolution Diffusion and Anatomical MRI Acquisition

2.2.1. MRI Sample Preparation

Well-fixed mouse brains were transferred to a custom-made MRI holder immersed in Fomblin-Y (perfluoropolyether, Milipore Sigma, HVAC 18/8, average molecular weight 1,800) to eliminate susceptibility artifact at the air-tissue interface and background proton signals. High-resolution MRI was acquired on a Bruker Biospec 7T/30 system (Bruker Biospin MRI, Billerica, MA) with a 35-mm quadrature coil for both signal transmission and reception. Two mouse brains are scanned at the same time.

2.2.2. High-Resolution 3D Isotropic Diffusion MRI Acquisition

High-resolution 3D isotropic diffusion MRI images were acquired with spin echo diffusion preparation, field of view (FOV)= 40 mm x 11 mm x 11 mm, acquisition matrix = 256 x 70 x 70, voxel size = 0.003796 mm³, repetition time (TR) = 1000 ms, echo time (TE) = 16.665ms, diffusion gradient duration (d) = 4 ms, diffusion gradient separation (D) = 8ms, diffusion directions = 30, b = 1200 s/mm².

2.2.3. High-Resolution 3D Isotropic Anatomical MRI

High-resolution 3D anatomical MRI was acquired for co-registration of diffusion MRI to the atlas space. 3D T₂-weighted isotropic anatomical MRI was acquired with 3D Rapid Imaging with Relaxation Enhancement (RARE), a Fast Spin-Echo (FSE) sequence, with exactly the same geometry as the diffusion scans, for anatomical registration in the same brain space with the following parameters: FOV = 40mm x 11mm x 11mm, matrix size = 512 x 141 x 141, TR = 1000ms, TE = 12 ms, RARE factor = 8, effective TE = 48 ms, refocusing flip angle 180 degrees.

2.3. Mouse Brain Template

Two *ex vivo* mouse brains underwent Diffusion MRI at the same time, so each diffusion-weighted imaging (DWI) Nifti volumes contained two mouse brains. The first volume of the DWI data was used to detect each mouse brain via watershed segmentation and a manually guided segmentation approach. Based on this segmentation for multiple mouse brains, the DWI data of each animal was stored in separate 4D Nifti files.

2.4. Atlas-Based segmentation

We have established an automatic atlas-based segmentation pipeline for mouse brains. The 3D volumes of high-resolution RARE anatomical MRI (Figure 1C) and diffusion MRI (Figure 1A) are first registered to the Allen mouse brain atlas[64–66] space as described previously[67] using ANTx2, a custom MATLAB toolbox and segmented into gray matter (GM), white matter (WM) and cerebrospinal fluid (CSF) tissue maps using the Unified Segmentation approach[68] as implemented in statistical parametric maps (SPM)[69]. For the segmentation task, the tissue probability maps (TPMs) are generated based on Hikishima et al.[70] tissue classification. A weighted image is constructed using the tissue segments of the animal and the TPMs of the template, respectively. The weighted images are co-registered using affine and nonlinear B-spline transformation via Elastix package[71]. The resulting parameters for forward transformation are stored to allow a subsequent image transformation from native animal space to mouse template space. Parameter files for inverse transformation are also generated and stored to allow a subsequent image transformation from template space to native space (e.g. hemispheric brain mask). Using the files for inverse transformation, we transform the template to the native, 1st volume of the 3D data to create the final brain segmentation mask. Each mouse brain is parcellated into 72 regions without assigning any region of interest (ROI) or region of avoidance (ROA). Abbreviations for each brain region are listed in Table S1.

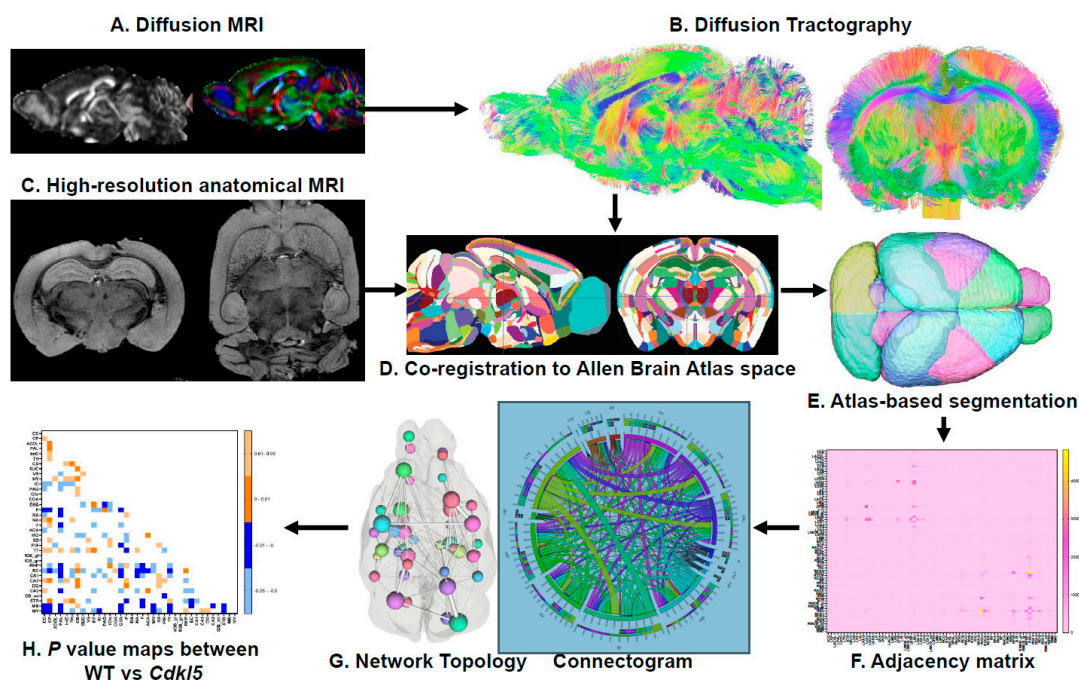


Figure 1. Flow diagram of diffusion MRI tractography and high-definition brain network (HDBN) delineation (A) Representative images of diffusion MRI. (B) High-definition 3D diffusion tractography generated from diffusion MRI. (C) Parallel acquisition of high-resolution T₂-weighted anatomical MRI with the same geometry as diffusion MRI. (D) Co-registration of diffusion tractography and high-resolution anatomical MRI the Allen brain atlas space to perform (E) Atlas based segmentation. (F) Adjacency matrix that is generated from a combination of tractography through various regions of the atlas-based segmentation. (G) Brain topology and connectogram generated from adjacency matrix. (H) Group comparisons between WT and *Cdk15* KO mice to generate *p* value matrix for brain region connectivity that are significantly different in the adjacency matrices.

2.5. Diffusion Tractography

Quantification of fiber tracking (Figure 1B) was completed using DSI studio June 2018 version, with a minimum fiber track length of 0, maximum fiber track length 300 mm, tracking algorithm RK4, angular threshold 0, and a total of 1,000,000 seeds calculated using a 0.07710 threshold. These parameters were used for whole brain seeding, left hemisphere fiber tracking, and right hemisphere fiber tracking. Seeds were placed on an entire hemisphere and the corresponding hemisphere atlas added to see where of the 36 regions the fiber tracts mapped. This allowed us to assess the amount of fiber tracts in each region. The process was repeated for the right hemisphere. We investigated both the ipsilateral and contralateral fiber tracking to see if the left and right hemispheres were comparable. For the contralateral tracking, seeds were placed in the left hemisphere and compared to the right hemisphere's fiber numbers. This was then repeated with the opposite hemispheres. After performing the ipsilateral and contralateral fiber tracking, we ultimately found them to not be significant and instead combined both into whole brain fiber tracking. The whole brain fiber tracking was performed on predetermined regions of interest that consisted of cerebellum, entorhinal cortex, hippocampus, hypothalamus, medulla, somatomotor cortex, somatosensory cortex, superior colliculus, thalamus, and visual cortex. Of these, the hippocampus region was made by combining the CA1, CA2, CA3, and dentate gyrus (DG) regions and the isocortex region was used for the visual cortex. The whole brain tract rendering was set to local index and either FA, MD, AD, or RD (Table S2) on a heat scale of 0-1 in DSI studio. The fiber track colors indicate their direction with red being left to right fibers, blue being front to back fibers, and green being top to bottom fibers.

2.6. Adjacency Matrix and Connectogram:

The hemisphere of the 72-region atlas-based parcellation used as the ROIs to create the adjacency matrices (Figure 1F) and connectograms (Figure 1G) depended on ipsilateral or contralateral analysis. For close-range fiber analysis, the hemisphere ipsilateral to where the seeds were placed of the 72-region atlas-based parcellation was used as the ROIs, and an adjacency matrix was calculated by using count of the connecting tracks in DSI studios after tractography. For long-range fiber analysis, the hemisphere contralateral to where the seeds were placed was used for calculation of the count of connecting tracts. The graph theory extraction threshold for both ipsilateral and contralateral was 0.001. In contralateral analysis, heat maps will display all 72x72 regions. Chord diagrams of adjacency matrices were generated using Circos table viewer (<http://circos.ca/>), where row and column size were matched creating ribbons that are to scale with the number of connections between two regions of interest, each color representing a different region. Graphs are undirected. Chord diagrams of contralateral data display cross hemisphere connections, either 36x36 left seeds to map tracks to right regions and vice versa, to avoid redundancy. Representative ball and stick plots are 3D graph visualizations in which balls represent nodes and sticks represent edges. The size of the ball corresponds to the number of connections in a brain region, and the width of the sticks is proportional in size to the number of edges between nodes. As such, these are visual representations of our network parameters.

2.7. Network Topography

Brain network topology was characterized for WT and *Cdkl5* mice following the previously described protocol[67]. Using the same tractography that made the adjacency matrices, graph theoretical analysis was calculated by DSI studio for various network parameters. The graph theory [72–74] extraction threshold was 0.001. These network parameters included measures of efficiency, global efficiency and small worldness, and measures of segregation, local efficiency, and clustering coefficient.

The process from imaging to network topology and connectogram are depicted in Figure 1. Characterizing neuronal networks into network measures through graph theory describes the physiological aspect of information processing, quantifying structure and function[75]. Network measures in DSI studio follow the implementation of the brain connectivity toolbox. Graph theoretical analysis treats brain connections like a graph, so its topology can be quantitatively described by network parameters. We graph weighted measures, such that the connectivity matrix will be normalized so the maximum value of the matrix is one.

2.8. Statistical Analysis

We performed multiple unpaired t-tests with corrections to assess the volume, FA, AD, MD, and RD of regional ROIs. For differences in fiber tracking, we used multiple unpaired t-tests at 95% confidence level. A P-value map was then generated showing the regional differences where the $p < 0.05$. A t-test was used for network parameters as well.

Differences between WT and KO brain connectivities were performed by comparing the distribution of fiber tracts in between all $36(36-1)/2=630$ pairs of brain regions. We excluded pairs where $>50\%$ of their observations were 0 and, to alleviate skewing and make the data more amenable to linear models, log-transformed the data after adding a pseudo count of 1 to avoid taking the log of zero. T-tests with $n_{WT} + n_{KO} - 2=17$ degrees of freedom were used to compare WT and KO pairs and resulting p-values (Figure 1H) were adjusted using the Benjamini Hochberg procedure to adjust for multiple testing by controlling the FDR at 5%[76]. These computations were performed in Rv4.1.2.

3. Results

3.1. Probing Brain Micro-Environment and Connectivity with Diffusion MRI and Diffusion Tractography

Diffusion MRI (Figure 1A) generating high-definition fiber tractography (HDFT, Figure 1B) is a non-invasive way to characterize brain micro-environment and to map neuronal connections in the entire brain. Diffusion MRI[44–52] leverages anisotropic water diffusion properties in the biological tissue to generate MRI contrast[53,54] sensitive to local structural or pathophysiological micro-environment. Neuronal fibers (axons, long dendrites) found in white matter tracks, fasciculi, and commissures are the long, slender projections of neurons that transmit electrical and chemical signals inter-connecting brain regions to form “information highway” networks that process information and conduct cognitive functions. There are also afferent (sensory) fibers and efferent (motor) fibers to carry information to and from the central nervous system (CNS) respectively, as well as autonomic fibers to relay information to regulate involuntary sympathetic and parasympathetic functions. In neuronal fibers, water molecules can readily diffuse along neuronal fiber orientation, but are very limited perpendicular to the neuronal fiber orientation due to diffusion barriers of cell membranes and myeline sheath[55–58]. Diffusion MRI leverages this anisotropic restricted water diffusion property in nerves to non-invasively map neuronal track orientations and connections in the brain. Diffusion tractography models water diffusion patterns in neuronal fibers as a Gaussian distribution and determination of axonal direction by the three principal directions of the tensor[44,45].

Although diffusion tensor imaging (DTI) is by far the most widely used diffusion MRI method, its major limitations have been well described[61–63], particularly its inability to represent the crossing of multiple fibers[77]. The diffusion tensor model assumes one dominant fiber orientation per voxel. This assumption fails when multiple fiber populations with different orientations are present, leading to misinterpretation of DTI metrics [61]. Mouse brains (~1 to 1.5 cm in length, ~0.4–0.5 cm³ in volume) are ~3,000 times smaller than human brains (~14 to 16 cm in length, ~1,200–1,400 cm³ in volume) [78–81]. Even with much smaller voxel sizes, conventional DTI[82–84] often fall short and cannot distinguish multiple fiber orientations within a voxel in small mouse brains. Several alternative advanced methods have been proposed to address this limitation[85]. Here we use high-angular generalized q-sampling imaging (GQI)[86] with deterministic fiber tracking for this study[50,87,88], optimized for small mouse brains.

GQI[86] is a model-free reconstruction method that quantifies the density of diffusing water at different orientations. This measurement, termed spin distribution function (SDF), is an orientation distribution function of diffusing spins. Studies have shown its greater sensitivity and specificity to white matter characteristics and pathology[89–91]. GQI can calculate SDF from a variety of diffusion data sets[92,93], including DSI dataset, high angular resolution diffusion imaging (HARDI) [62,94,95], multiple-shell [96–98], or combined DTI datasets. GQI provides an analytical relation to compute SDF, and the reconstruction requires only a simple matrix multiplication.

The deterministic fiber tracking algorithm makes use of the local fiber orientations to delineate the whole trajectory. It starts from a seeding point and propagates along fiber orientation until the termination criteria are met. Examples of this approach include the fiber assignment continuous tracking (FACT) method[50] and streamline fiber tracking algorithm[46], both of which assume a single fiber orientation per voxel. With high angular resolution data, multiple fiber orientations can be resolved per voxel to catch the complex connections of the fiber geometry[87,99,100], more suitable for small mouse brains.

By quantifying the tensors for these principal directions, the trajectories of the axonal connections can be tracked by diffusion fiber tractography, which reveals the axonal orientations and connections between brain areas[59,60]. Eigenvalues of each tensor direction (λ_1 , λ_2 , λ_3) can quantify diffusivity (Table S2) for each brain region, sensitive to the local micro-structure and micro-environment, thus they can reflect neurodevelopmental and pathophysiological features[101–103]. Fractional anisotropy (FA)[44] quantifies the degrees of anisotropy (non-uniformity) of water diffusion in neuronal fibers. FA represents the degree to which diffusion within a voxel-of-interest is isotropic or anisotropic, with a value of 0 representing the former and 1 representing the latter FA is a fraction derived from the ratio between λ_1 , λ_2 , and λ_3 . It has a value ranged from 0 (isotropic) to 1 (totally anisotropic). FA reflects neuronal fiber integrity and coherency. Axial diffusivity (AD) [102]

measure diffusion along the axonal orientation, which can reflect axonal integrity and or axonal injury. AD, denoted by $\lambda_{\text{parallel}}$, quantifies how fast water diffuses along the axonal fibers[104–106]. It is estimated by λ_1 , the first eigenvalue of the tensor. Radial diffusivity (RD)[102] measure diffusion perpendicular to the axonal orientation, reflecting myeline integrity. RD, denoted by $\lambda_{\text{perpendicular}}$, quantified how fast water diffuses across the axonal bundles. It is estimated by $(\lambda_2+\lambda_3)/2$, the average of the second and third eigenvalues of the tensor. It can be used to study demyelination[107]. Mean diffusivity (MD), or apparent diffusion coefficient (ADC), measures overall diffusivity for all directions[102]. MD is the diffusivity average from the three eigenvalues of the tensor. It is often regarded as an approximation of the overall ADC.

Quantitative diffusivity (FA, AD, RD, MD) are sensitive to micro-environment and micro-structure, thus providing a non-invasive way to probe the pathophysiological and neurodevelopmental features in live brains. Numerous studies have investigated the relation between diffusivity and pathological conditions. For example, axonal injury, traumatic injury, stroke, amyotrophic lateral sclerosis (ALS), advanced multiple sclerosis (MS) can increase AD, demyelination can increase RD, a tumor can decrease MD, immune cell infiltration has decreased MD. Vasogenic edema increases MD/ADC whereas cytotoxic edema decreases MD/ADC. Age-dependent changes in AD, RD, and MD during neurodevelopment are well recognized[108–110]. Developing brains rapidly change axonal characteristics in axonal density, axonal caliber, and myelination[108–110]. Diffusive parameters can be used to characterize brain maturation in pre-term infants[111–114] which showed gestation-age dependent and brain-region specific changes in AD, RD, and MD. Children with dyslexia[115–117] showed changes in these diffusivity parameters. Thus, quantitative diffusivity are increasingly used as biomarkers for white matter for neurodevelopment[108–110], brain maturation[111–114], cognitive abilities[115–117], brain injury[118–122], and neurodegeneration[123–126].

Diffusion MRI was successful in detecting selective vulnerability of the frontal lobes in Rett Syndrome[127]. It is conceivable that quantitative diffusivity might be able to quantify brain changes in CDD to provide a non-invasive quantitative brain-based biomarker for CDD trials.

We first investigated quantitative diffusivity in hemizygous male *Cdkl5* KO mouse brains compared to those of the age- and sex-matched WT counterparts (Figure 2). Group-averaged quantitative diffusivity mapping covers 3D volumes of the entire brain. They can be viewed in any orientation for each brain region, allowing visual comparison between WT and *Cdkl5* KO mice. Figure 2 shows a mid-sagittal view of the 3D isotropic mapping of group-averaged FA (Figure 2A-C), MD (Figure 2D-F), AD (Figure 2G-I), and RD (Figure 2J-L) maps for WT (Figure 2 A, D, G, J) and *Cdkl5* KO mice (Figure 2B, E, H, K) as well as the *p* value maps (Figure 2 C, F, I, L, and Table S3) for group comparisons between the hemizygous male *Cdkl5* KO mice and the WT counterparts. A two-sample unpaired t-test was used to determine the brain regions with significant differences between the two groups (Figure 2 C, F, I, L, and Table S3).

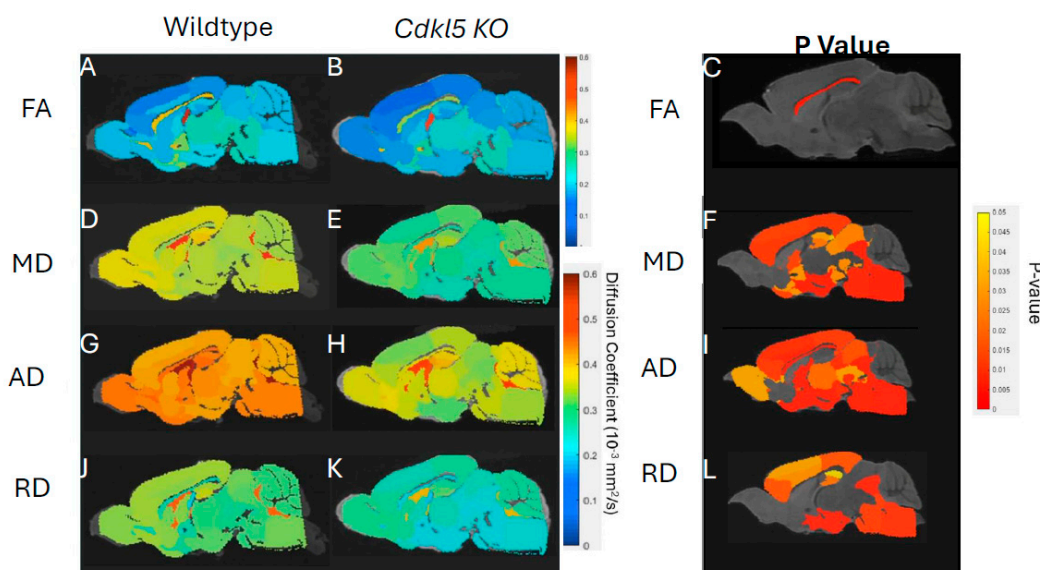


Figure 2. Group comparison of quantitative diffusivity (A) Representative images of whole brain have been rendered on a scale of 0–0.6 for average fractional anisotropy (FA), medial diffusivity (MD), axial diffusivity (AD), and radial diffusivity (RD) per ROI. General patterning of FA appears to be the same between WT and *Cdk15*, but different patterning for MD, AD, and RD. (B) Representative images highlighting regions that are significantly different according to the t-test.

Cdk15 KO mice showed significant changes in FA in the corpus callosum (Figure 2C), the colossal white matter gateway for communicating between the left and right hemispheres. This is consistent with the observation that CDKL5 sculpts functional callosal connectivity to promote cognitive flexibility[128].

MD (Figure 2F), AD (Figure 2I), and RD (Figure 2L) were altered in the somatosensory and somatomotor cortex, hippocampus, amygdala, hypothalamus, superior colliculus, pons, and other subcortical regions (Table S3). Somatosensory and somatomotor cortex are crucial for cognitive functioning and decision-making, hippocampus[129–132] for contextual learning and memory, amygdala[133–137] for anxiety- and fear-like responses, hypothalamus for homeostasis, pons for connecting to spinal cord, and superior colliculus[138–140] for visual/motor functions involving in processing optical stimuli, orienting attention, and coordinating hand-eye movements. We found that the brain regions showed significant different diffusivity in *Cdk15* KO mice are consistent with clinical symptoms in CDD patients. This suggests that brain-region specific quantitative diffusivity mapping can potentially be brain-based biomarkers for CDD.

Our data showed that quantitative diffusivity with diffusion MRI can sensitively detect micro-environmental changes in *Cdk15* KO mice. The brain areas with significant changes correlated with the brain regions underlying cognitive disabilities found in CDD patients.

3.2. Global High-Definition Fiber Tractography (HDFT):

Next, we compared streamlines of the 72 regions on a whole brain level. The high-definition fiber tractography (HDFT Figure 1B) and high-resolution anatomical T₂-weighted MRI (Figure 1C) were first co-registered to the Allen Brain Atlas[64–66] space (Figure 1D) for atlas-based segmentation (Figure 1E) to parcellate each mouse brain into 72 brain regions.

The diffusion parameters (Figure 2, Table S3) showed significant differences in many regions between *Cdk15* and WT mice. We investigated if the neuronal fiber numbers were also altered. To do this, the numbers of diffusion streamlines passing through each brain region for each mouse were generated, then the group mean streamline numbers are compared between *Cdk15* and WT mice using

a two-sample unpaired t-test adjusting for FDR at 5%. The average numbers of diffusion streamlines, reflecting the total neuronal fibers, were significantly altered in several regions of *Cdkl5* mice (Table S4, highlighted brain regions), including corpus callosum (LCC), cerebellum (LCB), motor related superior colliculus (LSUC), hypothalamus (LHY), inferior colliculus (LIC), amygdala (LCOA), somatomotor cortex (LMO), somatosensory cortex (LSS), piriform cortex (LPIR), taenia tecta (LTT), retrohippocampal region (LRHP), and mid-brain (LMB). Each of the altered brain regions are responsible for different cognitive functions – cortex[141,142] involved in executive functions, hippocampus[143–148] in contextual learning, amygdala[133–137] in anxiety and fear conditioning, cerebellum[149,150] in motor functions, piriform cortex [151,152] for olfactory processing, hypothalamus [153,154] for homeostasis, autonomic regulation, emotional expression, and stress responses, whereas the motor related superior colliculus[155–157] transforms sensory and cognitive signals into motor commands for saccadic eye movements and coordination of eye–head–body movements. These altered brain regions carrying out cognitive functions correlated with clinical presentations of CDD patients[1–12], such as intellectual disabilities; anxiety and irritability; circadian rhythm dysregulation and sleep disturbances; autonomic dysfunctions; visual and cortical visual impairments with poor visual tracking and reduced eye contact; hypotonia and motor abnormalities with spasticity, dystonia, or poor motor coordination.

Our data demonstrated that *Cdkl5* mutant mice exhibited region-specific alterations in diffusion-derived streamline density, a proxy for neuronal fiber numbers, within brain regions implicated in the cognitive impairments characteristic to CDD clinical manifestation.

3.3. Brain Topology with High-Definition Brain Network (HDBN) Analysis:

We further characterize the brain topology in *Cdkl5* brains using graph theory. Brain topology[75,158–160] refers to the organizational principles of the brain's structural or functional networks, describing how neural elements (e.g., neurons, neuronal populations, or brain regions) are interconnected, formalized using graph theory[74,158,161,162], in which brain regions are modeled as nodes and their anatomical or functional connections as edges. This framework enables quantitative characterization of global and local network properties that govern information integration, segregation, and robustness of brain systems. Graph theory provides a powerful mathematical framework for delineating brain network architecture by representing the brain as a complex system of interconnected elements and enabling quantitative characterization of its organization across multiple spatial scales. In this framework, nodes typically correspond to anatomically or functionally defined brain regions, while edges represent structural or functional connections between nodes, derived from diffusion tractography. Topological features of brain networks include measures such as density, clustering coefficient, path length, global or local efficiency, and small-worldness, which collectively capture how efficiently information is transferred and processed across the brain. Alterations in brain topology have been widely reported in neurodevelopmental, neuropsychiatric, and neurodegenerative disorders, suggesting that disrupted network organization is a core mechanism underlying cognitive and behavioral impairments.

Here we investigate if disruption of the brain network architecture underlies neurocognitive impairments in CDD. Adjacency matrices (Figure 1F) represent interconnections among 72 brain regions. Adjacency matrices (Figure 1F) capturing interregional connectivity among 72 brain regions were aggregated across individual mice within the WT or *Cdkl5* cohorts to generate group-level connectogram (Figure 1G, right), which is a circular graphical representation that visualizes the structural or functional connectivity between brain regions, depicting nodes as regions and links as their pairwise connections. The brain topology can also be represented with the ball-and-stick model (Figure 1G, left), which is a simplified network representation in which brain regions are modeled as nodes (“balls”) and their structural or functional connections are modeled as edges (“sticks”), allowing the topological organization of the brain (e.g., hubs, modules, and small-world properties) to be analyzed using graph theory.

To compare connectivity between WT and *Cdkl5* KO brains, we performed two-sample unpaired t-test for pair-wise comparisons of the distribution of fiber tracts in between all $36(36-1)/2=630$ pairs of brain regions, aggregating among all individual brains to generate the adjusted p value matrix (Figure 1H), using the two-step adjusted p values with signs. The lighter colors represent $|p|$ values are between 0.01-0.05, whereas the darker colors represent $|p|$ values between 0 - 0.01. Although p values do not have signs, we artificially assign “positive” or “negative” denotations to indicate the direction of deviations of *Cdkl5* brains from the WT brains. The blue colors denote artificially assigned “negative” p values, indicating *Cdkl5* KO brains have less connections than WT brains, whereas the orange colors denote artificially assigned “positive” p values, indicating *Cdkl5* KO brains have more connections than the WT counterparts. The adjusted p value matrix can compare shorter pair-wise connections within the hemispheres (ipsilateral) or longer range pair-wise connections to the other hemisphere (contralateral). The topological analysis can be performed at the whole brain levels or for each sub-circuitry.

In brain network analysis using graph theory[163–167], brain network topological characteristics can be quantified by network parameters. Healthy brains typically exhibit a “small-world”[168–170] topology. The “**small-worldness**” in brain networks refers to a topological property where the brain’s connectivity graph shows both high local clustering (segregation) and short average path lengths (global integration), supporting efficient information processing compared to random networks. In neuroscience, it’s quantified by comparing the clustering coefficient and path length of a real brain network to those of equivalent random graphs, with a *small-world index* (σ) > 1 indicating small-world characteristics in structural and functional connectomes. The “**path length**” refers to the average shortest number of edges that must be traversed to connect any two nodes, reflecting the efficiency of information transfer across the network. Shorter path lengths indicate faster global communication between brain regions, while longer path lengths suggest less efficient connectivity. The “**clustering coefficient**” is a measure in network theory that quantifies how “clustered” or “connected” a node’s neighbors are. In other words, it tells you the likelihood that two nodes that are both connected to a common node are also connected to each other. It is commonly used in social networks, brain networks, and other complex networks to describe local connectivity. The “**global efficiency**” measures the ability of the network to integrate information across the whole brain. It quantifies how efficiently signals can travel between any pair of nodes in the network. The “**local efficiency**” measures how efficiently information is exchanged within the immediate neighborhood of a node. It reflects the fault tolerance of the network — how well communication is preserved if a node is removed. The “**density**” is a measure of how many connections (edges) exist in a network relative to the maximum possible number of connections. For a brain network, nodes typically represent brain regions, and edges represent structural (e.g., white matter tracts) or functional (e.g., correlated activity) connections. High density can mean that brain regions are highly interconnected; the network is more integrated, whereas low density usually means fewer connections relative to possible ones, indicating that the brain network is sparser. “**Transitivity**” is a measure of the tendency for nodes (brain regions) to form triangles, reflecting the likelihood that two neighbors of a node are also connected. It’s a global measure of clustering in the network. Essentially, high transitivity indicates tightly interconnected modules or communities in the brain. The “**assortativity coefficient**” measures the tendency of nodes (brain regions) to connect to other nodes that are similar in some property, most commonly degree (number of connections). If the assortativity coefficient is positive, high-degree nodes tend to connect to other high-degree nodes (and low-degree to low-degree), showing a “like-with-like” connectivity pattern. If it is negative, high-degree nodes tend to connect to low-degree nodes, indicating disassortative mixing. If it is near zero, connections are roughly random with respect to node degree. In brain networks, assortativity can indicate network resilience and organization. Positive assortativity suggests robustness against random damage because highly connected hubs are interconnected. Negative assortativity often occurs in biological networks where hubs connect to peripheral nodes, which can optimize communication efficiency. In graph theory applied to brain networks, a “**rich club**” refers to a set of highly connected hub nodes

that are more densely interconnected with each other than expected by chance. These nodes typically have a high degree of connections and form a “club” of influential regions that facilitate efficient communication and integration across the brain. The “rich club” organization of the brain supports global integration, efficient information transfer, and resilience to localized damage.

3.4. Data-Driven Network Topology Characterization of *Cdkl5* KO Brains

We first characterize brain network topology in *Cdkl5* KO brains by data-driven approach. Our data found significant changes in diffusion parameters (Figure 2, Table S3) and diffusion streamlines (Table S4) which reflect the numbers of neuronal fibers in Cerebellum, Superior Colliculus, Hippocampus, Thalamus, Entorhinal Cortex, Hypothalamus, Medulla, Motor Cortex, and Somatosensory Cortex. All these areas carry out cognitive functions that are characteristic of CDD clinical manifestations. We delineate network topology in these brain regions.

3.4.1. Network Topology Changes in *Cdkl5* at the Whole Brain Level

Brain topological analysis at the whole brain level (Figure 3 and Table S5) found extensive changes in many pairs of connections for the *Cdkl5* group. While *Cdkl5* brains showed many brain connections deviated from those in WT counterparts (blue or orange colors in p value matrixes in Figure 5G-J), many brain connections are normal (blank in the p value matrixes in Figure 5G-J). None of the brain network parameters by graph theory at the whole brain level (small-worldness, path length, clustering coefficient, global efficiency, local efficiency, density, transitivity, assortativity coefficient, or rich clubs, etc) showed significant differences between *Cdkl5* KO and WT brains. This indicates that *Cdkl5* brain network changes are region-specific in local circuitries, not at the global whole brain level.

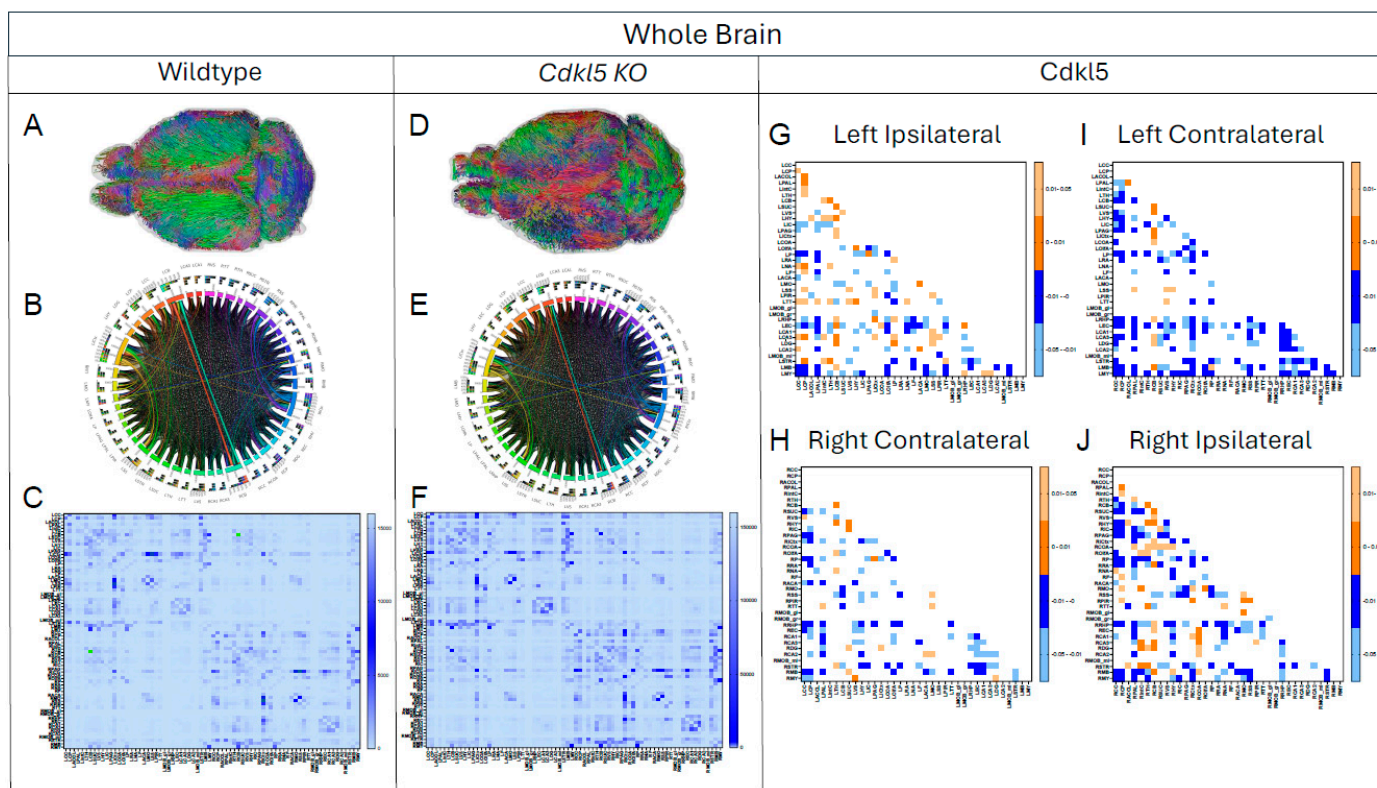


Figure 3. Diffusion tractography and brain network analysis for the whole brain (A, B) Diffusion tractography (B, E) connectogram (C, F) adjacency matrix for WT (A-C) or hemizygous *Cdkl5* KO mice (D-F). (G-J) P value matrix to compare connectomes, an adjacency matrix of signed FDR adjusted p-values shows connections between regions where *Cdkl5* KO > WT (0.01-0.05 light orange, 0.005-0.01 dark orange) and connections between

regions where $WT > Cdkl5$ KO (0.0- -0.05 light blue, -0.005- -0.01 dark blue) for (G) left ipsilateral hemisphere connections (left to left hemisphere), (H) right contralateral connections (right to left hemispheres) (I) left contralateral connections (left to right hemispheres) and (J) right ipsilateral hemisphere connections (right to right hemisphere).

3.4.2. Regional Network Topology Changes in *Cdkl5* Brains

We then characterized regional brain network topology in brain regions that showed significant changes in diffusion parameters (Figure 2, Table S3) and diffusion streamlines (Table S4) which reflect the numbers of neuronal fibers, including Cerebellum (Figure 4, Table S6), Superior Colliculus (Figure 5, Table S7), Hippocampus (Figure 6, Table S8), Thalamus (Figure 7, Table S9), Entorhinal Cortex (Figure 8, Table S10), Hypothalamus (Figure 9, Table S11), Medulla (Figure 10, Table S12), Motor Cortex (Figure 11, Table S13), and Somatosensory Cortex (Figure 12, Table S14). All these areas carry out cognitive functions that are characteristic of CDD clinical manifestations. All these brain areas showed varied degrees of altered brains short-ranged in the ipsilateral hemispheres (Figure 4-12, G, J) as well as in the long-ranged contralateral hemispheres (Figure 4-12, H, I). Contrary to the whole brain network topology, all these brain regions showed changes in brain network parameters. Hypothalamus (Figure 9L) showed changes in small-worldness. Entorhinal Cortex (Figure 8M) and IsoCortex (Figure 13N) showed changes in path length. Superior Colliculus (Figure 5K), Medulla (Figure 10K), and IsoCortex (Figure 13L) showed changes in clustering coefficient. Hypothalamus (Figure 9N) and Medulla (Figure 10L) showed changes in global efficiency. Hypothalamus (Figure 9M) and Medulla (Figure 10M) also showed changes in local efficiency. Hippocampus (Figure 6K), Thalamus (Figure 7K), Entorhinal Cortex (Figure 8K), Hypothalamus (Figure 9K), Motor Cortex (Figure 11K), Somatosensory Cortex (Figure 12K), and IsoCortex (Figure 13K) showed changes in density. Superior Colliculus (Figure 5L), Entorhinal Cortex (Figure 8L), and Medulla (Figure 10N) showed changes in transitivity. Cerebellum (Figure 4K), Entorhinal Cortex (Figure 8N), and IsoCortex (Figure 13M) showed changes in assortativity coefficient. The regional brain network topological analysis indicates that *Cdkl5* deficiency leads to regional brain network alterations in brain-region specific manners.

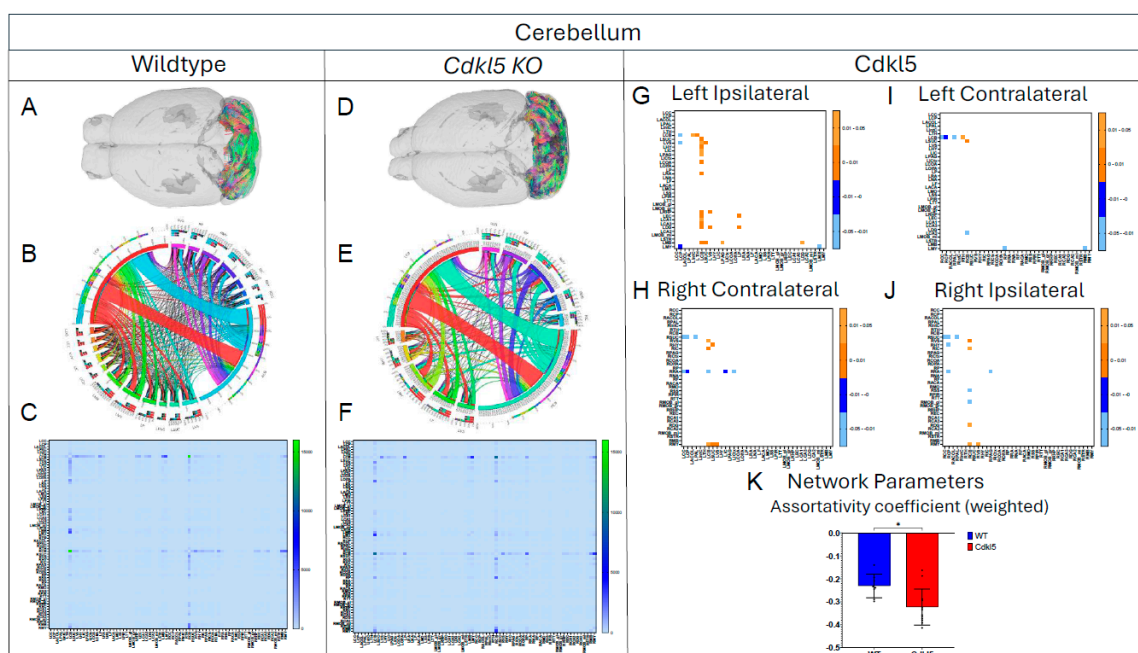


Figure 4. Diffusion tractography and brain network analysis for cerebellum. (A, B) Diffusion tractography (B, E) connectogram (C, F) adjacency matrix for WT (A-C) or hemizygous *Cdkl5* KO mice (D-F). (G-J) P value matrix to compare connectomes, an adjacency matrix of signed FDR adjusted p-values shows connections between

regions where *Cdkl5* KO > WT (0.01-0.05 light orange, 0.005-0.01 dark orange) and connections between regions where WT > *Cdkl5* KO (0.0- -0.05 light blue, -0.005- -0.01 dark blue) for (G) left ipsilateral hemisphere connections (left to left hemisphere), (H) right contralateral connections (right to left hemispheres) (I) left contralateral connections (left to right hemispheres) and (J) right ipsilateral hemisphere connections (right to right hemisphere). (K) Network parameter - Assortativity coefficient (weighted). Blue – WT, Red – *Cdkl5* KO. .

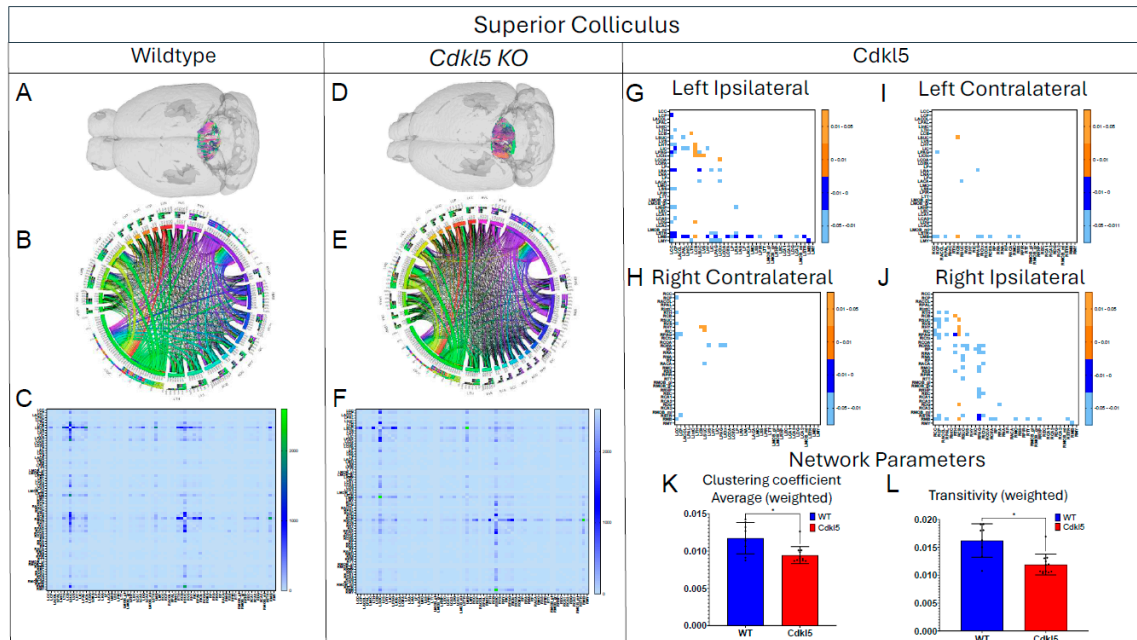


Figure 5. Diffusion tractography and brain network analysis for Superior Colliculus. (A, B) Diffusion tractography (B, E) connectogram (C, F) adjacency matrix for WT (A-C) or hemizygous *Cdkl5* KO mice (D-F). (G-J) P value matrix to compare connectomes, an adjacency matrix of signed FDR adjusted p-values shows connections between regions where *Cdkl5* KO > WT (0.01-0.05 light orange, 0.005-0.01 dark orange) and connections between regions where WT > *Cdkl5* KO (0.0- -0.05 light blue, -0.005- -0.01 dark blue) for (G) left ipsilateral hemisphere connections (left to left hemisphere), (H) right contralateral connections (right to left hemispheres) (I) left contralateral connections (left to right hemispheres) and (J) right ipsilateral hemisphere connections (right to right hemisphere). (K-L) Network parameters, (K) Clustering coefficient (weighted) (L) Transitivity (weighted). Blue – WT, Red – *Cdkl5* KO. .

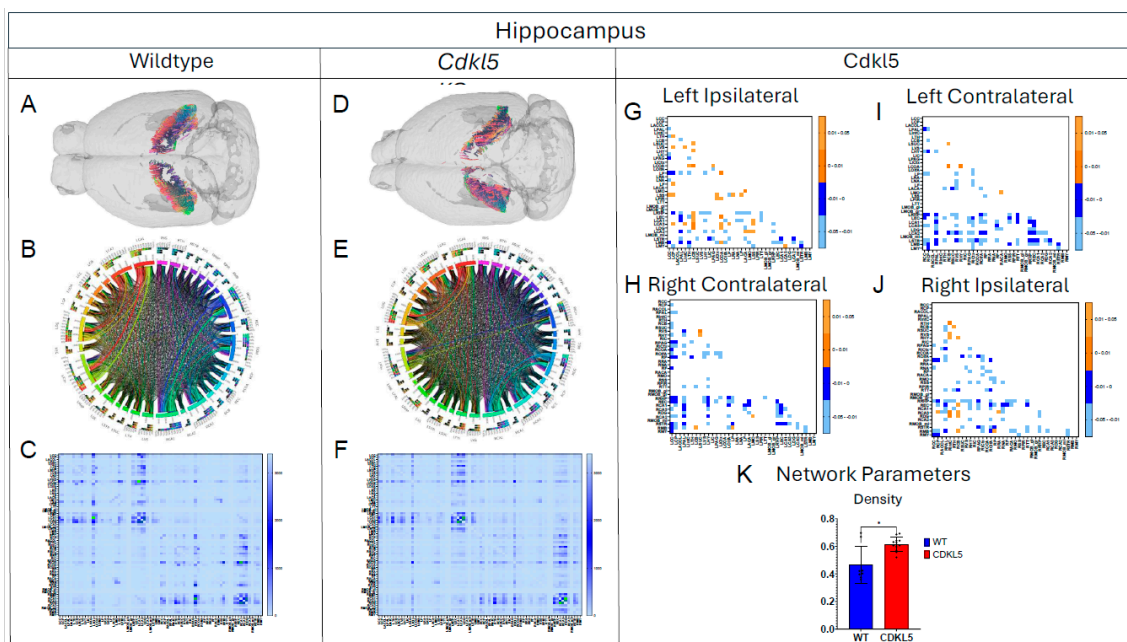


Figure 6. Diffusion tractography and brain network analysis for Hippocampus. (A, B) Diffusion tractography (B, E) connectogram (C, F) adjacency matrix for WT (A-C) or hemizygous *Cdkl5* KO mice (D-F). (G-J) P value matrix to compare connectomes, an adjacency matrix of signed FDR adjusted p-values shows connections between regions where *Cdkl5* KO > WT (0.01-0.05 light orange, 0.005-0.01 dark orange) and connections between regions where WT > *Cdkl5* KO (0.0- -0.05 light blue, -0.005- -0.01 dark blue) for (G) left ipsilateral hemisphere connections (left to left hemisphere), (H) right contralateral connections (right to left hemispheres) (I) left contralateral connections (left to right hemispheres) and (J) right ipsilateral hemisphere connections (right to right hemisphere). (K) Network parameter – Density. Blue – WT, Red – *Cdkl5* KO .

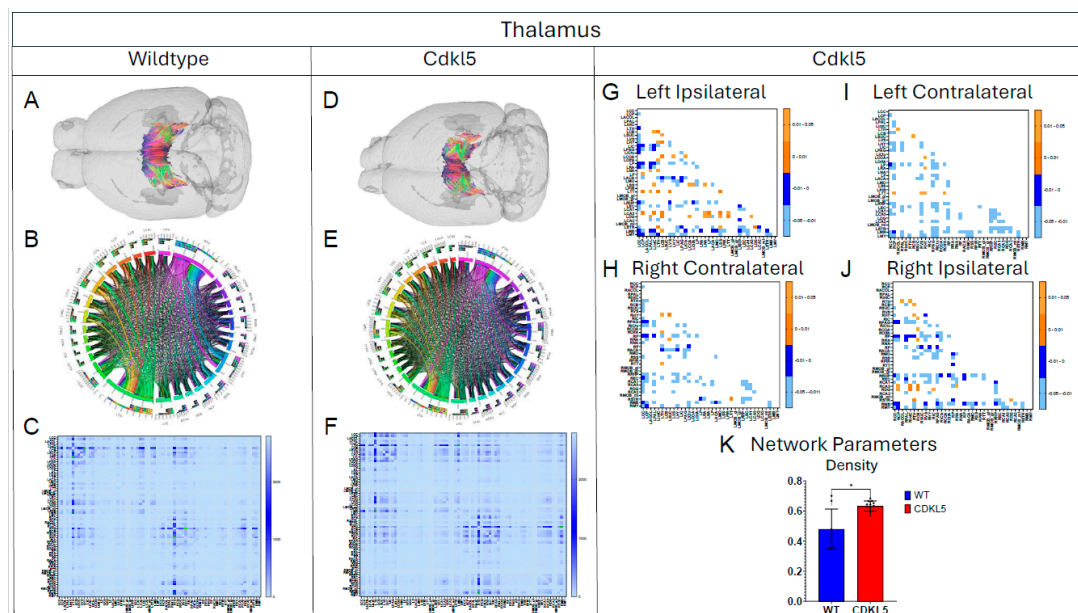


Figure 7. Diffusion tractography and brain network analysis for Thalamus. (A, B) Diffusion tractography (B, E) connectogram (C, F) adjacency matrix for WT (A-C) or hemizygous *Cdkl5* KO mice (D-F). (G-J) P value matrix to compare connectomes, an adjacency matrix of signed FDR adjusted p-values shows connections between regions where *Cdkl5* KO > WT (0.01-0.05 light orange, 0.005-0.01 dark orange) and connections between regions where WT > *Cdkl5* KO (0.0- -0.05 light blue, -0.005- -0.01 dark blue) for (G) left ipsilateral hemisphere connections (left to left hemisphere), (H) right contralateral connections (right to left hemispheres) (I) left contralateral

connections (left to right hemispheres) and (J) right ipsilateral hemisphere connections (right to right hemisphere). (K) Network parameter – Density. Blue – WT, Red – *Cdk15* KO. .

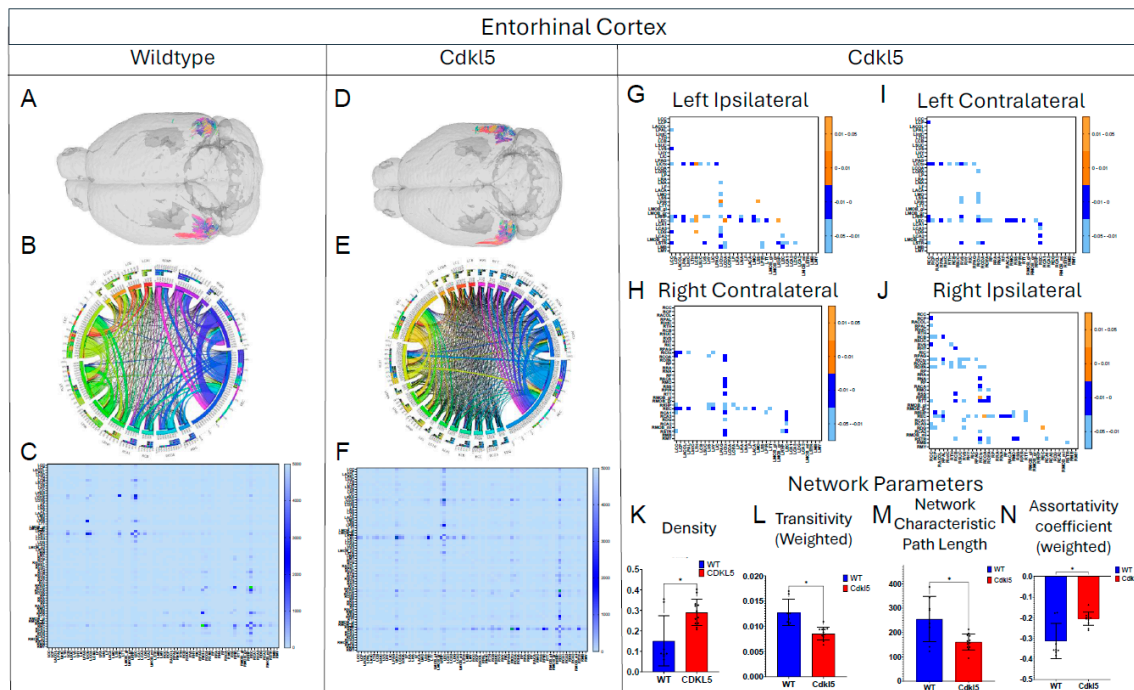


Figure 8. Diffusion tractography and brain network analysis for Entorhinal Cortex. (A,B) Diffusion tractography (B, E) connectogram (C, F) adjacency matrix for WT (A-C) or hemizygous *Cdk15* KO mice (D-F). (G-J) P value matrix to compare connectomes, an adjacency matrix of signed FDR adjusted p-values shows connections between regions where *Cdk15* KO > WT (0.01-0.05 light orange, 0.005-0.01 dark orange) and connections between regions where WT > *Cdk15* KO (0.0- -0.05 light blue, -0.005- -0.01 dark blue) for (G) left ipsilateral hemisphere connections (left to left hemisphere), (H) right contralateral connections (right to left hemispheres) (I) left contralateral connections (left to right hemispheres) and (J) right ipsilateral hemisphere connections (right to right hemisphere). (K-N) Network parameter (K) Density, (L) Transitivity (weighted), (M) Path length, (N) Assortativity coefficient (weighted). Blue – WT, Red – *Cdk15* KO. .

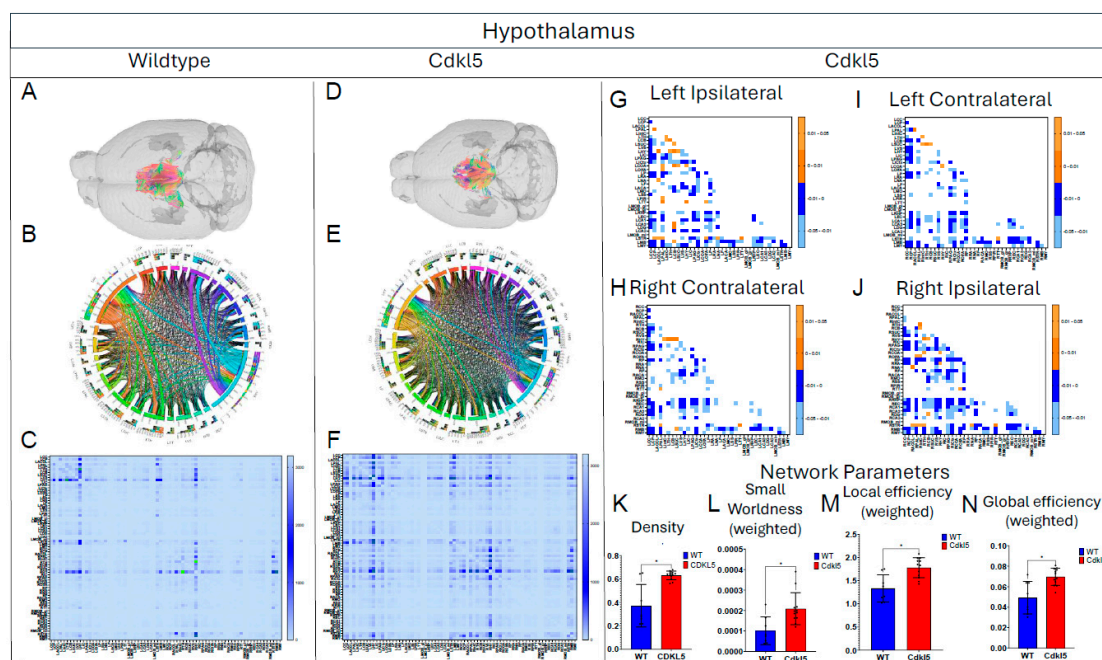


Figure 9. Diffusion tractography and brain network analysis for Hypothalamus. (A, B) Diffusion tractography (B, E) connectogram (C, F) adjacency matrix for WT (A-C) or hemizygous *Cdkl5* KO mice (D-F). (G-J) P value matrix to compare connectomes, an adjacency matrix of signed FDR adjusted p-values shows connections between regions where *Cdkl5* KO > WT (0.01-0.05 light orange, 0.005-0.01 dark orange) and connections between regions where WT > *Cdkl5* KO (0.0- -0.05 light blue, -0.005- -0.01 dark blue) for (G) left ipsilateral hemisphere connections (left to left hemisphere), (H) right contralateral connections (right to left hemispheres) (I) left contralateral connections (left to right hemispheres) and (J) right ipsilateral hemisphere connections (right to right hemisphere). (K-N) Network parameter (K) Density, (L) Small worldness (weighted), (M) Local efficiency (weighted), (N) Global efficiency (weighted). Blue – WT, Red – *Cdkl5* KO. .

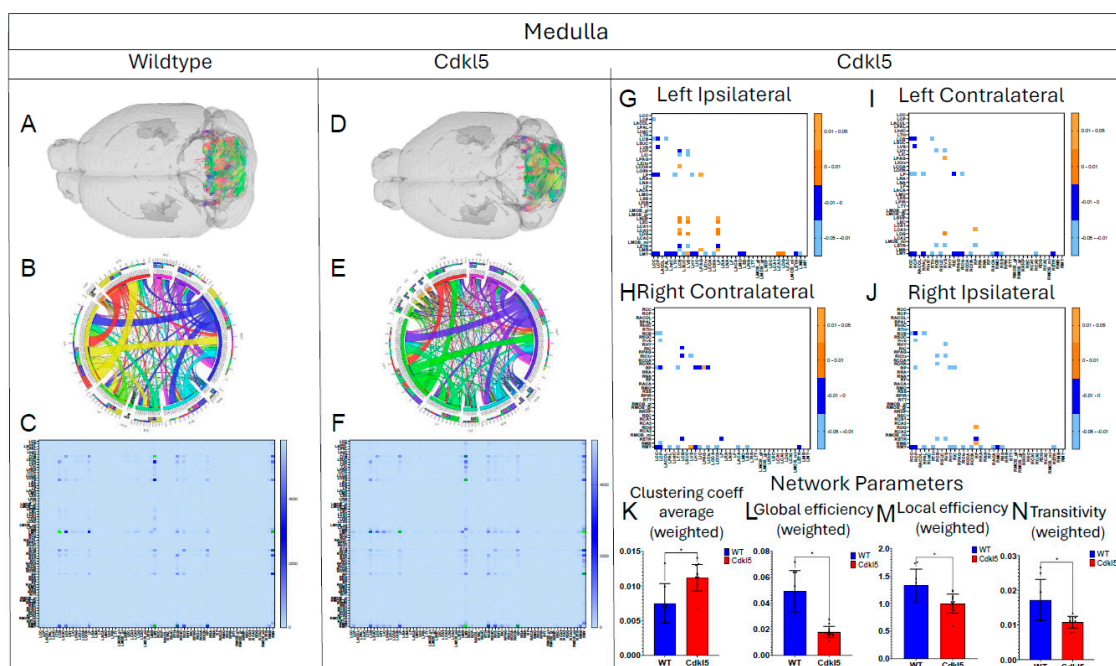


Figure 10. Diffusion tractography and brain network analysis for Medulla. (A, B) Diffusion tractography (B, E) connectogram (C, F) adjacency matrix for WT (A-C) or hemizygous *Cdkl5* KO mice (D-F). (G-J) P value matrix to compare connectomes, an adjacency matrix of signed FDR adjusted p-values shows connections between regions where *Cdkl5* KO > WT (0.01-0.05 light orange, 0.005-0.01 dark orange) and connections between regions where WT > *Cdkl5* KO (0.0- -0.05 light blue, -0.005- -0.01 dark blue) for (G) left ipsilateral hemisphere connections (left to left hemisphere), (H) right contralateral connections (right to left hemispheres) (I) left contralateral connections (left to right hemispheres) and (J) right ipsilateral hemisphere connections (right to right hemisphere). (K-N) Network parameter (K) Clustering coefficient, (L) Global efficiency, (M) Local efficiency, (N) Transitivity. Blue – WT, Red – *Cdkl5* KO. .

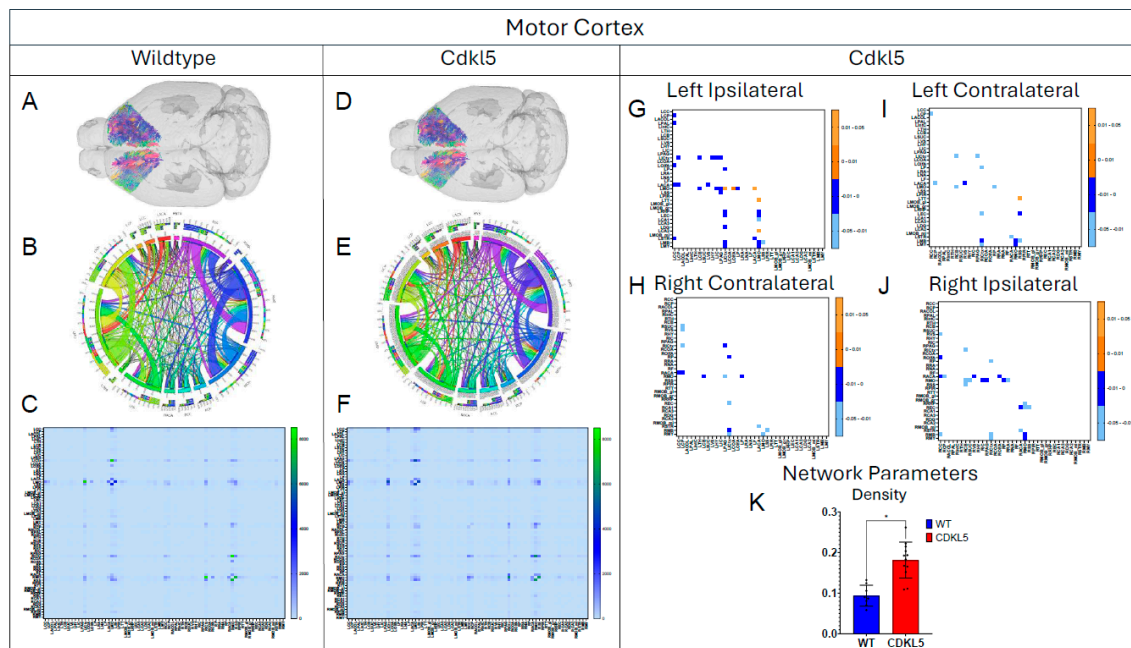


Figure 11. Diffusion tractography and brain network analysis for Motor Cortex. (A, B) Diffusion tractography (B, E) connectogram (C, F) adjacency matrix for WT (A-C) or hemizygous *Cdkl5* KO mice (D-F). (G-J) P value matrix to compare connectomes, an adjacency matrix of signed FDR adjusted p-values shows connections between regions where *Cdkl5* KO > WT (0.01-0.05 light orange, 0.005-0.01 dark orange) and connections between regions where WT > *Cdkl5* KO (0.0- -0.05 light blue, -0.005- -0.01 dark blue) for (G) left ipsilateral hemisphere connections (left to left hemisphere), (H) right contralateral connections (right to left hemispheres) (I) left contralateral connections (left to right hemispheres) and (J) right ipsilateral hemisphere connections (right to right hemisphere). (K) Network parameter – Density. Blue – WT, Red – *Cdkl5* KO. .

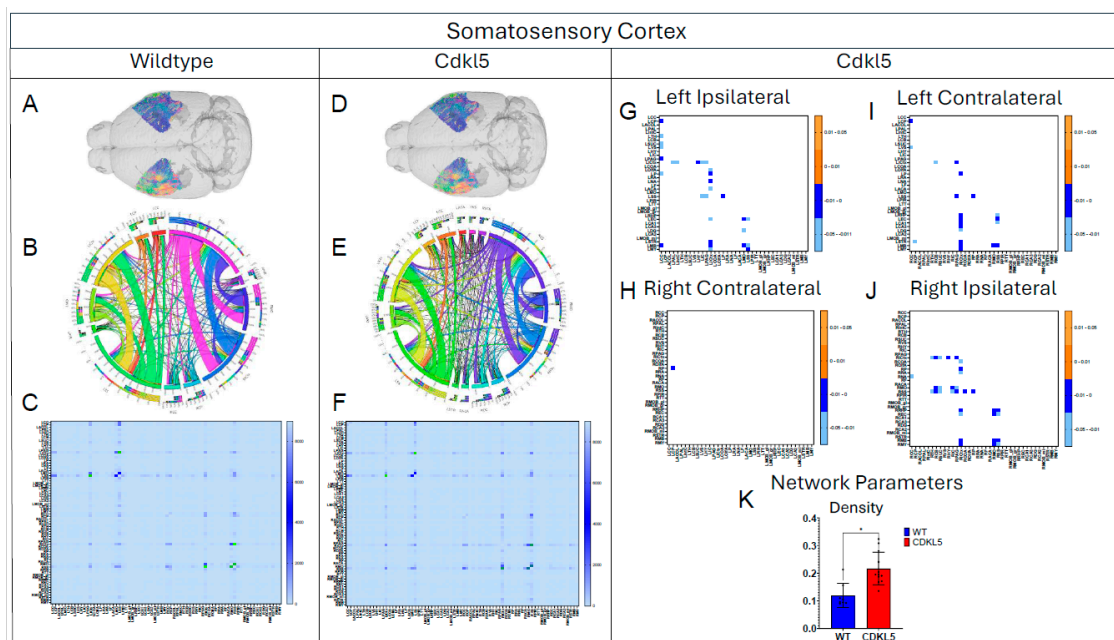


Figure 12. Diffusion tractography and brain network analysis for Somatosensory Cortex. (A, B) Diffusion tractography (B, E) connectogram (C, F) adjacency matrix for WT (A-C) or hemizygous *Cdkl5* KO mice (D-F). (G-J) P value matrix to compare connectomes, an adjacency matrix of signed FDR adjusted p-values shows connections between regions where *Cdkl5* KO > WT (0.01-0.05 light orange, 0.005-0.01 dark orange) and connections between regions where WT > *Cdkl5* KO (0.0- -0.05 light blue, -0.005- -0.01 dark blue) for (G) left ipsilateral hemisphere connections (left to left hemisphere), (H) right contralateral connections (right to left hemisphere), (I) left contralateral connections (left to right hemispheres) and (J) right ipsilateral hemisphere connections (right to right hemisphere). (K) Network parameter – Density. Blue – WT, Red – *Cdkl5* KO. .

hemispheres) (I) left contralateral connections (left to right hemispheres) and (J) right ipsilateral hemisphere connections (right to right hemisphere). (K) Network parameter – Density. Blue – WT, Red – *Cdkl5* KO. .

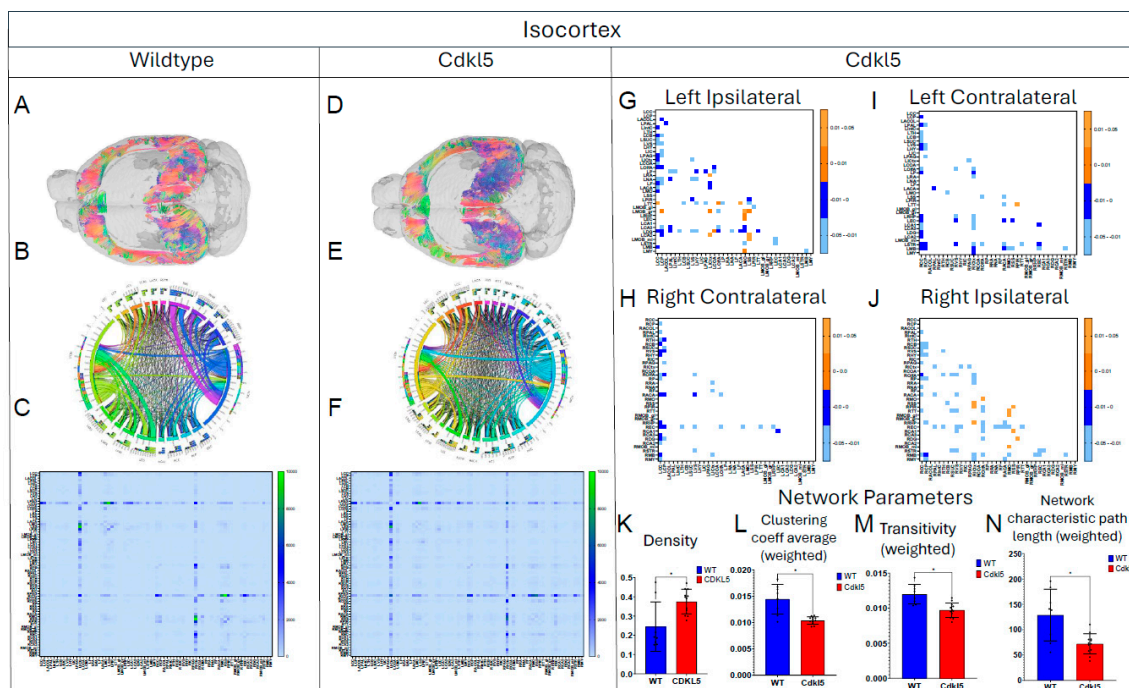


Figure 13. Diffusion tractography and brain network analysis for IsoCortex. (A, B) Diffusion tractography (B, E) connectogram (C, F) adjacency matrix for WT (A-C) or hemizygous *Cdkl5* KO mice (D-F). (G-J) P value matrix to compare connectomes, an adjacency matrix of signed FDR adjusted p-values shows connections between regions where *Cdkl5* KO > WT (0.01-0.05 light orange, 0.005-0.01 dark orange) and connections between regions where WT > *Cdkl5* KO (0.0- -0.05 light blue, -0.005- -0.01 dark blue) for (G) left ipsilateral hemisphere connections (left to left hemisphere), (H) right contralateral connections (right to left hemispheres) (I) left contralateral connections (left to right hemispheres) and (J) right ipsilateral hemisphere connections (right to right hemisphere). (K-N) Network parameter (K) Density, (L) Clustering coefficient (M) Transitivity, (N) Network characteristic path length (weighted). Blue – WT, Red – *Cdkl5* KO. .

3.5. Hypothesis-Driven Characterization of Brain Circuitry for CDD

We then characterize brain circuitry indicated by clinical presentations of CDD patients, in particular, circuitry for anxiety and fear related behavior (3.5.1) and hippocampal-thalamic projection in the temporal lobe epilepsy (3.5.2).

3.5.1. Brain Network Characterization in the Fear Conditioning Circuitry

CDD patients can show anxiety and fear-related behaviors with increased irritability, anxiety and fear-related behavior, and emotional dysregulation, which suggests potential amygdala dysfunction. *Cdkl5* KO mice[36] displayed similar behavioral phenotypes with significant increases in anxiety- and fear-related responses, as well as hypervigilance. *Cdkl5* KO mice performed poorly in various rodent behavioral testing paradigms, including the fear conditioning[34]. The neuronal circuitry for amygdala-dependent fear conditioning[171] has been uncovered, which involves neuronal pathways (Figure 14 A) from the external stimulation to thalamus (TH, Figure 14A orange), somatosensory cortex (SS, Figure 14A, dark blue), isocortex (ICtx, Figure 14A, purple), hypothalamus (HY, Figure 14A, light blue), and amygdala (CoA, Figure 14A, green). We characterized the neuronal connections between these brain regions in WT (Figure 14B-G, and Figure 15 blue) and *Cdkl5* KO brains (Figure 14 H-M, and Figure 15 red). Neuronal connections between isocortex and thalamus, (Figure 15A, ICtx-TH), amygdala and thalamus (Figure 15B COA-TH), between amygdala and hypothalamus (Figure 15D, COA-HY), and between amygdala and isocortex (Figure 15E, COA-

ICtx) in the ipsilateral hemispheres are significantly altered in *Cdk15* KO mice compared to the WT counterparts. This indicates that the maladapted neuronal circuitry underlies the behavioral deficits of fear conditioning paradigm in *Cdk15* KO mice. On the other hand, long-range connections of these areas to the contralateral hemispheres (Figure 15 G-L) are not different. This suggests that the neurocognitive deficits of fear conditioning arisen from local neuronal circuitry not from the long-range inter-hemisphere connections.

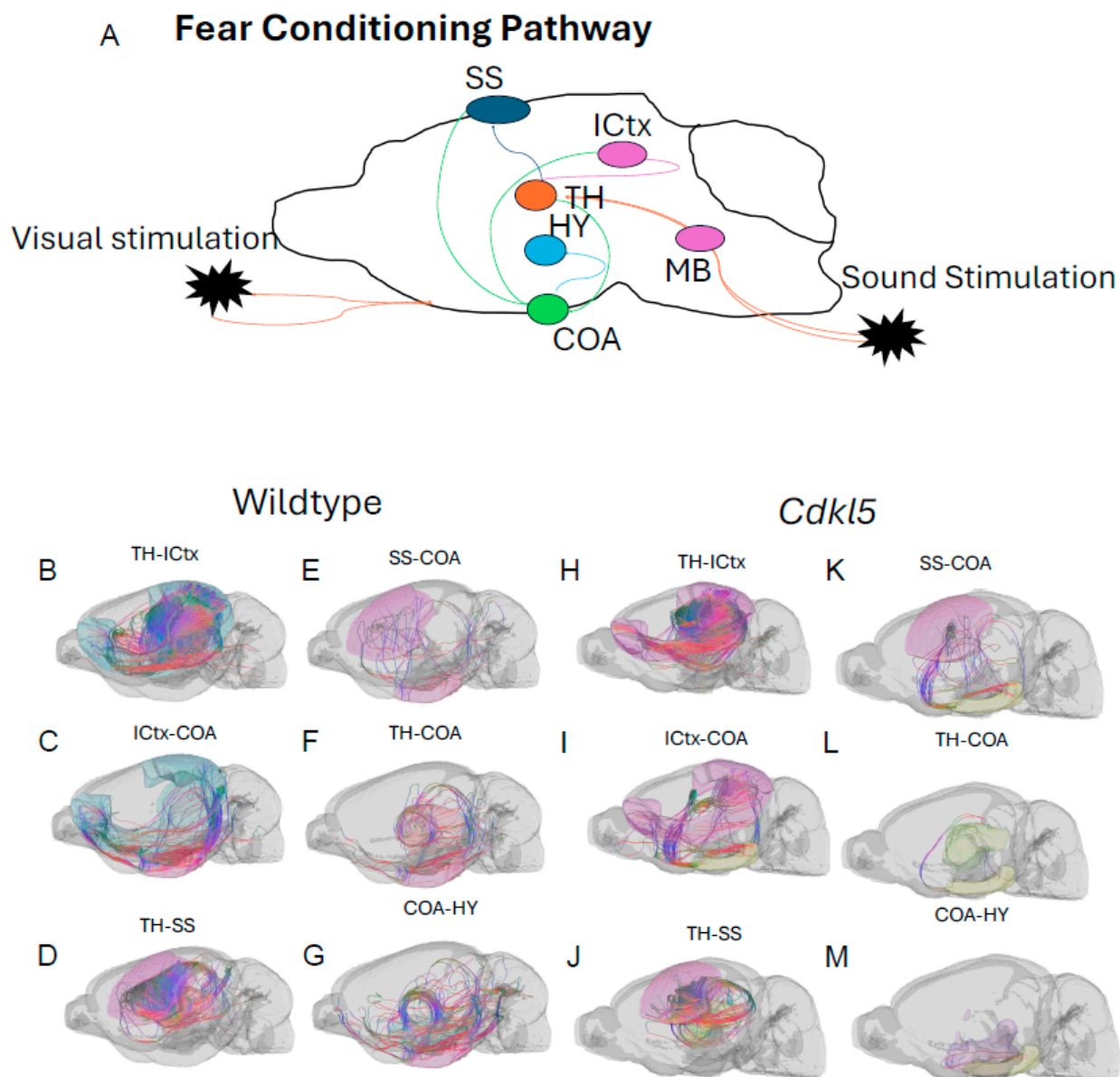
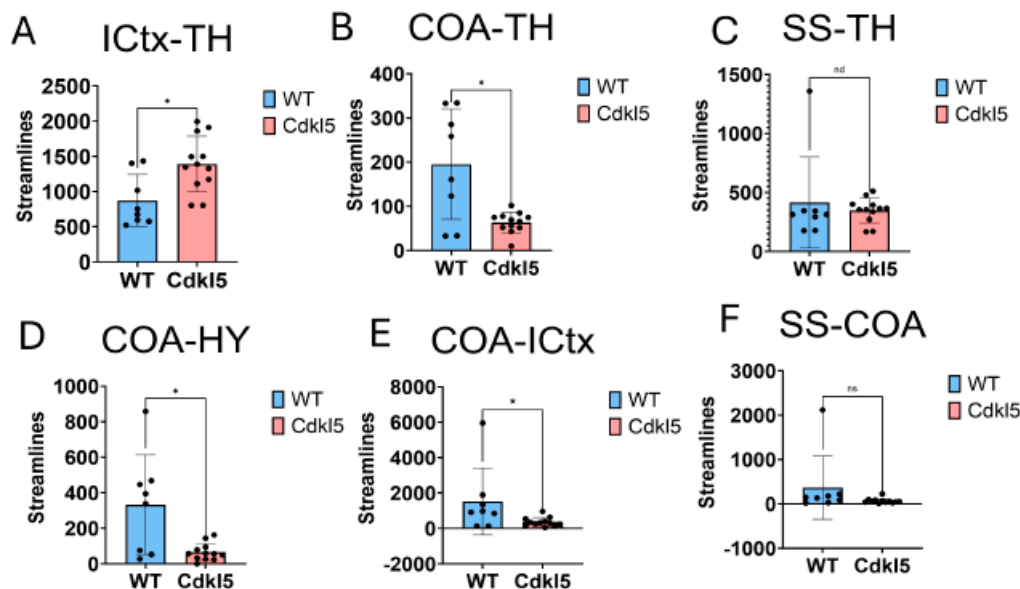


Figure 14. Diffusion tractography and brain network analysis for the fear conditioning pathway. (A) Diagram of fear conditioning pathway from Visual stimulation through the optic track and through sound stimulation to midbrain, Thalamus (TH), hypothalamus (HY), amygdala (CoA), somatosensory cortex (SS) and Isocortex (ICtx). (B-M) Diffusion tractography for (B-G) WT and (H-M) *Cdk15*, for connections between TH-ICtx (B, H), ICtx-COA (C, I), TH-SS (D, J), SS-COA (E, K), TH-COA (F, L), COA-HY (G, M).

Fear Conditioning Ipsilateral Streamlines



Fear Conditioning Contralateral Streamlines

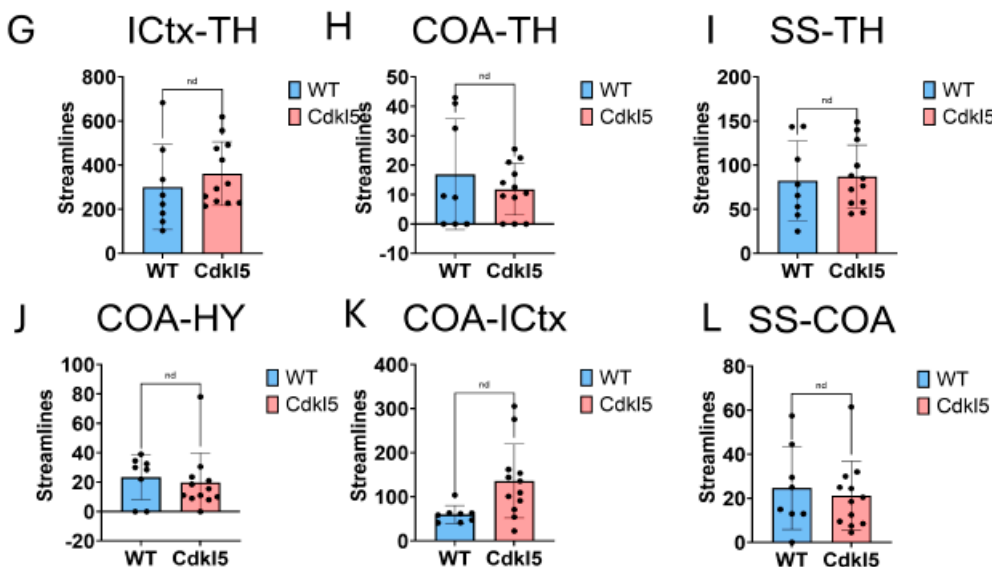


Figure 15. Diffusion tractography and brain network analysis for the fear conditioning. (A-F) Group averaged connections in Ipsilateral connections (G-L) or the Contralateral connections (S-X) for ICtx-TH (A, G), COA-TH (B, H), SS-TH (C-I), COA-HY (D, J), COA-ICtx (E, K), SS-COA (F, L). Blue – WT, Red – *Cdk15* KO.

3.5.2. Brain Network Characterization of Circuitry in the Temporal Lobe Epilepsy

Majority of CDD patients suffer from refractory epilepsy with frequent seizures that cannot be controlled by current ASMs. Temporal lobe epilepsy (TLE) [172] is the most common focal epilepsy and often involves complex alterations in neuronal pathways. Understanding the circuitry helps explain seizure generation, propagation, and associated cognitive/emotional symptoms. In addition to key brain regions involved in TLE, such as hippocampus (Figure 16A blue), entorhinal cortex (Figure 16A orange), amygdala (Figure 16A, light pink), and isocortex (Figure 16A, lavender), the hippocampal (Figure 16A blue)–thalamic (Figure 16A green) pathway [173–175] is critically involved in both seizure propagation and modulation. Thalamus is a target for surgery [176] or deep brain stimulation (DBS) [177,178] to treat drug-resistant TLE. Furthermore, thalamus [179–181] is a crucial brain structure for sensory relay, motor integration, cognitive and emotional processing, and

regulation of consciousness, wakefulness and sleep rhythms. These functions are often impaired in CDD patients.

Here we characterize the TLE and hippocampal–thalamic pathway in *Cdkl5* mice (Figs. 16, 17). The neuronal connections between hippocampus and isocortex (Figure 17D Hipp-ICtx), entorhinal cortex and amygdala (Figure 17E EC-CoA), and hippocampus and amygdala (Figure 17F, Hipp-CoA) are significantly altered in the ipsilateral hemisphere. However, surprisingly, the hippocampal–thalamic connections (Figure 17A, Hipp-TH) and hippocampal–entorhinal cortex connections (Figure 17G, Hipp-EC) remain largely unchanged. Similar to the fear conditioning circuitry, the long-range TLE connections to the contralateral hemispheres remain the same. This again indicates the re-wiring of the local circuitry.

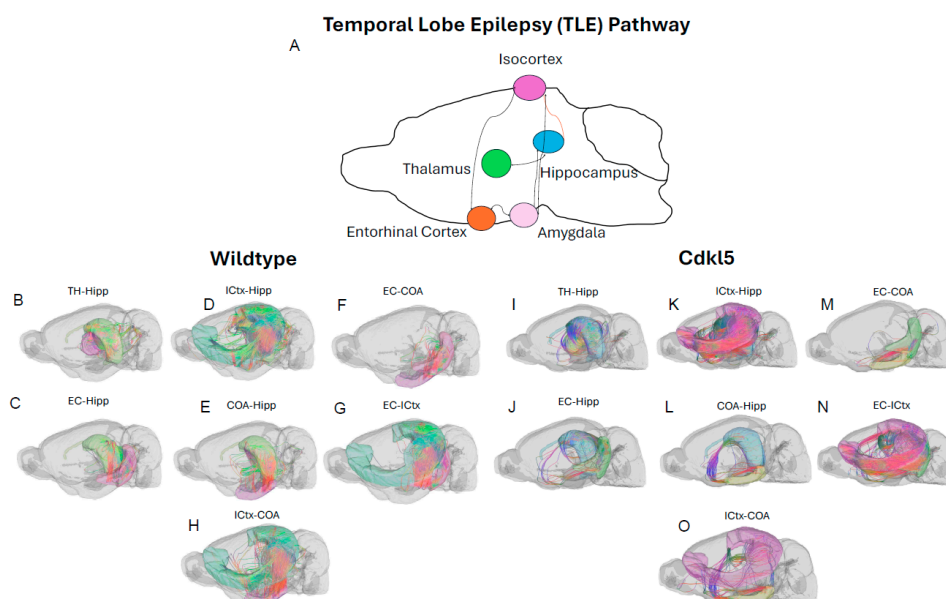


Figure 16. Diffusion tractography and brain network analysis for temporal lobe epilepsy (TLE). (A) Diagram of temporal lobe epilepsy pathways from hippocampus (blue) to thalamus (green), isocortex (dark pink), amygdala (light pink), or entorhinal cortex (orange). (B-O) Diffusion tractography for (B-H) WT and (I-O) *Cdkl5*, for connections between thalamus and hippocampus (B, I), entorhinal cortex-hippocampus (C, J), isocortex-hippocampus (D, K), amygdala-hippocampus (E, L), entorhinal cortex - amygdala (F, M), entorhinal cortex - isocortex (G, N) and isocortex - amygdala (H, O).

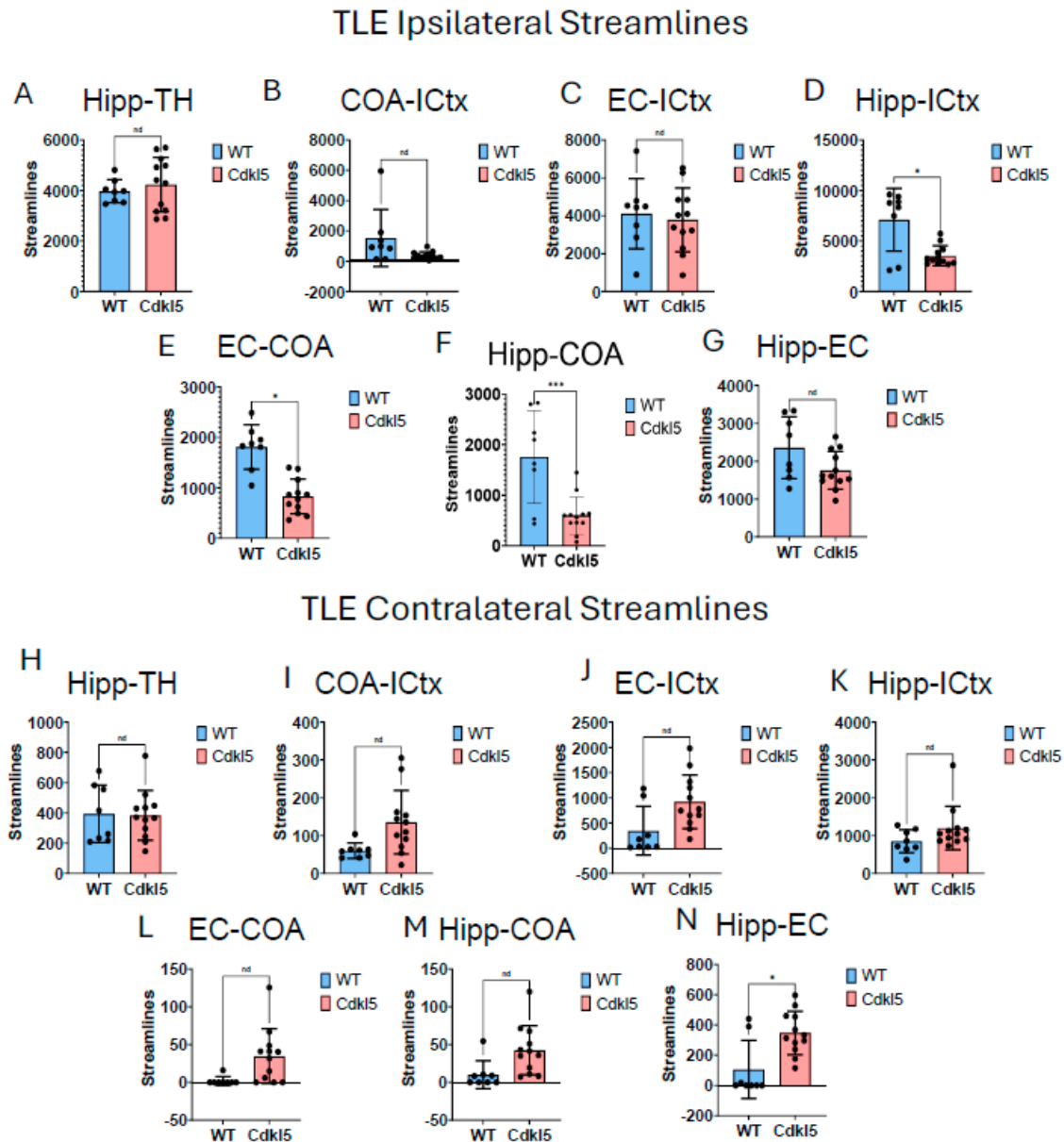


Figure 17. Diffusion tractography and brain network analysis for temporal lobe epilepsy.(M-X) Group averaged TLE connections in left hemisphere (M-R) or right hemisphere (S-X) for hippocampus-somatomotor cortex (M, S), hippocampus-somatosensory cortex (N,T), hippocampus-thalamus (O, U), somatomotor cortex - thalamus (P, V), somatosensory cortex-thalamus (Q, W), somatosensory-somatomotor cortex (R, X). Blue – WT, Red – *Cdk15* KO.

4. Conclusions and Discussion

Although some CDD patients do have abnormal brain structures, most CDD patients have unremarkable anatomical MRI in the first year of life [182]. In a study of male cohorts, brain MRI was completely normal in ~38% of cases [183]. CDD patients did not show reduced cortical volumes until later in age [182,184]. Similar to most CDD patients, *Cdk15* KO mice showed largely normal gross brain anatomy with no significant cerebral atrophy or gross structural abnormalities detectable on standard MRI scans, except subtle regional changes[185,186]. Our study demonstrated that diffusion MRI can sensitively detect neurodevelopmental differences in hemizygous *Cdk15* KO mice. Although gross anatomy is largely normal, quantitative diffusivity (FA, AD, RD, MD) can sensitively detect regional alteration in *Cdk15* KO mice. The brain regions that showed altered quantitative

diffusivity correlated to the brain regions underlying clinical presentations of cognitive impairments of CDD patients. Our study showed that diffusion MRI is more sensitive than conventional anatomical MRI in detecting neurodevelopmental changes in *Cdkl5* KO mice, consistent with clinical observations in CDD patients[182–184].

Diffusion MRI can be non-invasively performed longitudinally in patients. Regional diffusion parameters (FA, AD, RD, MD) are quantitative thus can potentially be individual patient-specific brain-based biomarkers for differential diagnosis, to track CDD progression, and to monitor therapeutic efficacy for clinical trials. Although each diffusion parameter (FA, AD, RD, or MD) is non-specific and can be influenced by many pathological conditions related to demyelination, injury, inflammation, infections, etc., combined profiles of all diffusion parameters and brain-region specific patterning may better depict the specific brain changes in individual CDD patients. Furthermore, it can be used to aid precision medicine to monitor CDD progression and CDD repression with therapeutic interventions.

In addition to neurodevelopmental changes, some CDD patients have frequent refractory epilepsy that cannot be controlled by current ASMs. Prolonged seizures with excessive neuron excitation, such as status epilepticus, can lead to excess glutamate release, calcium overload, bioenergetic crisis, and excitotoxicity and metabolic stress resulting in regional brain injury and inflammation. This can acutely change diffusion MRI parameters. To avoid confounding diffusion MRI readouts, diffusion MRI should not be performed acutely after seizure episodes, but should wait until the acute seizure effects resolved for more accurate readouts.

Our data-driven approach that *Cdkl5* KO mice exhibit region-specific alterations in diffusion-derived streamline density, a proxy for neuronal fiber organization, within brain regions implicated in the cognitive impairments characteristic of CDKL5 deficiency disorder (CDD) and underlying neurobehavioral phenotypes in *Cdkl5* KO mice[34,128]. Our data-driven approach identified regional alterations that converged with known CDD neuropathology, particularly within the cerebellum and superior colliculus. *Cdkl5* KO mice exhibited significant changes in cerebellar fiber counts, consistent with human imaging studies implicating cerebellar dysfunction in CDD [187]. Notably, disruptions were observed not only in cerebellar afferent and efferent connectivity but also in fibers traversing the cerebellum, suggesting that *Cdkl5* loss impairs cerebellar hub-like integration and long-range information flow across distributed brain networks. The superior colliculus[188], a key node in visual processing [189], also showed marked network disruption, aligning with cortical-visual deficits reported in CDD patients [190]. *Cdkl5* KO mice displayed reduced incoming and outgoing connections but increased through-passing fibers, indicating a shift from active network participation toward passive conduit-like function. These changes were accompanied by decreased global clustering coefficient and transitivity, consistent with impaired local network segregation and reduced efficiency of sensorimotor integration. The hippocampus has been consistently implicated as a vulnerable region in individuals with CDD[187]; therefore, we examined hippocampal network organization in greater detail. To capture hippocampal-wide connectivity, we combined ROIs encompassing CA1, CA2, CA3, and the dentate gyrus into a single hippocampal node. Network analysis revealed pronounced alterations in hippocampal fiber connectivity in *Cdkl5* KO mice relative to WT controls, indicating disrupted integration of this region within the broader brain network. In addition to changes in fiber connectivity, we observed a significant increase in hippocampal network density in *Cdkl5* KO mice. This elevated density is consistent with prior reports of hippocampal enlargement in *Cdkl5*-deficient mice and may reflect aberrant circuit expansion, altered synaptic pruning, or compensatory reorganization of hippocampal circuitry associated with CDKL5 loss. The thalamus serves as a major integrative hub, relaying and modulating information across cortical and subcortical systems that support sensory processing, cognition, and motor control. In *Cdkl5* KO mice, thalamic network architecture was disrupted in multiple dimensions. Specifically, we observed a significant reduction in the number of fibers traversing the thalamus, accompanied by a marked decrease in thalamic network density. These findings suggest impaired thalamic connectivity and reduced network integration, potentially contributing to widespread circuit dysfunction in CDD.

Our study demonstrated that even though *Cdkl5* KO mouse brains appear to be structurally normal without overt anatomical abnormalities, the brain networks, “the information highways” of the brain, are wired very differently. We have successfully probed these changes in brain network development using high-definition brain network (HDBN) delineation in *Cdkl5* KO mouse brains. Our findings demonstrate that HDBN provides a sensitive and precise method for mapping brain network architecture in *Cdkl5* KO mice, allowing clear differentiation from WT controls. *Cdkl5* KO mice exhibited pronounced alterations in neuronal network organization across multiple key regions, including the somatosensory and somatomotor cortices, hippocampus, hypothalamus, amygdala, and superior colliculus. These regions are critically involved in cognition, learning and memory, regulation of homeostasis, anxiety and fear conditioning, and visual-motor function, respectively, correlated with neurocognitive phenotypes in *Cdkl5* KO mice[34,36,191,192]. The observed network disruptions in these areas closely parallel the clinical manifestations of CDD patients, who frequently present with cognitive and memory deficits[1–4], anxiety[193], and cortical visual impairments[190]. Notably, the entorhinal cortex, a central component of the olfactory circuitry, appeared largely unaffected, suggesting region-specific vulnerability in *Cdkl5* deficiency. Together, these results highlight both the utility of HDBN for sensitive detection of network-level brain abnormalities and the selective impact of *Cdkl5* loss on functional brain circuits relevant to CDD pathophysiology. This is indicative that CDD, as a developmental and epileptic encephalopathy (DEE), even without epilepsy in mice, the brain network developed abnormally in *Cdkl5* mice. This is similar to clinical observations that some CDD patients do not have frequent seizures, or some seizures can be controlled, but CDD patients still suffer from neurodevelopmental disabilities suggesting underlying brain network abnormalities. Our study suggests that HDBN characterizing brain network topology might be more appropriate and sensitive for depicting CDKL5 deficiency in the brains for both humans and mice. HDBN delineation can also enable utilizing *Cdkl5* KO mice for mechanistic understanding and therapeutic development despite lacking overt seizures.

Both CDD patients and *Cdkl5* KO mice displayed anxiety and fear-related behaviors suggesting amygdalar dysfunctions. Our hypothesis-driven characterization of brain circuitry for fear conditioning found significant alterations of amygdala-related connections, confirming phenotypical observations in *Cdkl5* mouse models and in clinical manifestation of CDD patients.

Our characterization of neural circuitry for TLE further demonstrates the maladaptive neuronal network development underlie cognitive challenges in CDD. TLE is the most frequent form of epilepsy in CDD. TLE[194–196] emerges from maladaptive circuitry within the mesial temporal lobe, particularly the hippocampus, entorhinal cortex, and amygdala. Hyperexcitability of pyramidal neurons, combined with loss of inhibitory interneurons, disrupts excitation–inhibition balance, while mossy fiber sprouting of dentate granule cells establishes recurrent excitatory loops that promote seizure initiation. The entorhinal cortex–hippocampus loop sustains epileptiform activity, and amygdalar interactions facilitate propagation and emotional manifestations. Hippocampal sclerosis, characterized by selective hippocampal neuronal loss, further remodels circuitry to favor hyperexcitability. Additional temporal neocortical and thalamic networks mediate seizure spread, producing complex partial or secondary generalized seizures. These findings highlight TLE as a network disorder[197–199] in which synaptic reorganization, interneuron loss, and aberrant connectivity converge to generate recurrent, self-sustaining epileptic activity. Surprisingly, we found that the hippocampal-thalamic pathway in *Cdkl5* KO mice was normal. Most CDD patients suffer from refractory epilepsy, predominantly TLE. Hippocampal-thalamus project is important in managing drug-resistant TLE. However, *Cdkl5* KO mice do not exhibit TLE. Our hypothesis-driven characterization of brain circuitry for the hippocampal-thalamic project found no changes in *Cdkl5* KO mice. *Cdkl5* KO mice have normal hippocampus-thalamus projection. This is consistent with the observed phenotypes for *Cdkl5* KO mice. Our data demonstrates that HDBN can be sensitive in testing hypothesis-driven brain circuitry delineation in CDD and other DEE.

Allen Brain Atlas are constructed based on *ex vivo* histology with very thin slices (100 μm sampling density) and 0.35 μm pixel resolution[200] yielding 461 brain regions[66], whereas MRI

voxels are 78 μm and 156 μm in size for anatomical and diffusion MRI respectively. Many Allen Brain Atlas brain regions are too small and below the detection threshold of MRI signal to noise ratio (SNR). Thus, we combined smaller brain regions in Allen Brain Atlas to form 72 ROIs used in our analysis. This yielded good SNR and robust and reproducible HDBN results.

Conventional DTI can fall short of resolving neuronal fibers in small mouse brains. Our study used model-free generalized q-sampling imaging (GQI)[86] with high angular resolutions and deterministic fiber tracking algorithm more optimal for high-definition fiber tractography in small mouse brains, having overcome the drawbacks of conventional DTI. In conjunction with topological analysis with graph theory, our study has successfully depicted the neuronal network architecture in *Cdkl5* KO mouse brains. Although *Cdkl5* KO mice do not exhibit over seizures as CDD patients, HDBN can sensitively depict neurodevelopmental changes in *Cdkl5* KO mice, providing a sensitive, robust, and quantitative means for using *Cdkl5* KO mice for preclinical therapeutic development.

Studies show that neurocognitive abnormalities due to CDKL5 deficiency can be reversible. Terzic et al.[201] demonstrated that post-developmental loss of CDKL5 in mice leads to abnormal neuronal morphology and behavioral deficits, but restoring CDKL5 expression later in life ameliorated these deficits and reversed many functional abnormalities. CDKL5 is important for maintaining neuronal functions beyond development [201,202]. Using a conditional rescue mouse model, restoration of *Cdkl5* expression[201] after the early stages of brain development significantly ameliorated CDD-associated behavioral deficits and normalized aberrant NMDA receptor-mediated signaling. These findings demonstrate that CDKL5 function is required not only during early neurodevelopment but also for the maintenance of mature neural circuit function. Importantly, the ability to reverse core behavioral and synaptic abnormalities following post-developmental gene restoration provides compelling evidence that key aspects of CDD pathophysiology remain plastic beyond early critical periods. Together, these results underscore the potential for disease modification rather than purely symptomatic treatment and support the existence of a broad therapeutic time window for interventions targeting CDKL5-related deficits. Restoration of cognitive and behavioral deficits later in life with CDKL5 suggests normalization of the brain network. HDBN can sensitively delineate and quantify normalization of the brain network with therapeutic interventions. Further studies to determine the time frame that HDBN changes after therapeutic intervention can facilitate applications to accelerate therapeutic development for CDD beyond neurodevelopment.

Abbreviation

CDKL5 – Cyclin-dependent kinase-like 5
CDD – CDKL5 Deficient Disorder
DEE – developmental and epileptic encephalopathy
ASM – anti-seizure medication
NDD – neurodevelopmental deficit
KO – Knock out
MRI – Magnetic Resonance Imaging
DTI – Diffusion Tensor Imaging
DWI – Diffusion weighted imaging
HDFT – High-definition Fiber Tractography
HDBN – High-definition Brain Network
ROI – Region of Interest
FOV – Field of View
TE – Echo Time
TR – Repetition Time
FA – Fractional anisotropy
AD – Axial diffusivity
RD – radial diffusivity

MD – mean diffusivity
 ADC – apparent diffusion coefficient
 RARE – Rapid Imaging with Relaxation Enhancement
 FAS – Fast Spin-Echo
 GQI – generalized q-sampling imaging
 SDF – spin distribution function
 TPM – tissue probability map
 SPM – statistical parametric maps
 GM – grey matter
 WM – white matter
 OLAW – Office of Laboratory Animal Welfare
 IACUC – Institutional Animal Care and Use Committee
 FDA – Food and Drug Administration
 GEM – genetically engineered mouse
 WT – wild type

Supplementary Materials: The following supporting information can be downloaded at the website of this paper posted on Preprints.org.

Author Contributions: **Dalton West:** Investigation, Methodology, Formal analysis, Software, Validation, Data curation, Writing – original draft; Writing – review & editing. **Noah W. Coulson:** Investigation, Methodology, Formal analysis, Software, Validation, Data curation, Writing – original draft; Writing – review & editing. **Devin R. E. Cortes:** Methodology, Formal analysis, Software, Writing – review & editing. **Kristina E. Schwab:** Data curation, Methodology, Formal analysis, Writing – review & editing. **Thomas Becker-Szurszewski:** Data curation, Methodology, Formal analysis, Writing – review & editing. **Sean Hartwick:** Data curation, Methodology, Formal analysis, Writing – review & editing. **Margaret C. Stapleton:** Methodology, Formal analysis, Writing – review & editing. **Gabriella M. Saladino:** Formal analysis, Writing – review & editing. **Cecilia W. Lo:** Writing – review & editing. **Christina M. Patterson:** Writing – review & editing. **Subramanian Subramanian:** Writing – review & editing. **Deepa S. Rajan:** Writing – review & editing. **Yijen L. Wu:** Conceptualization, Investigation, Methodology, Formal analysis, Software, Validation, Data curation, Project administration, Funding acquisition, Supervision, Writing – original draft, Writing – review & editing.

Funding:

Institutional Review Board Statement: Animal protocols were approved by the University of Pittsburgh Institutional Animal Care and Use Committee (IACUC Protocol # 25066689, valid until June 4th, 2028).

Informed Consent Statement: Not applicable.

Data Availability Statement: The datasets are available from the corresponding author upon reasonable request.

Acknowledgments : This study was supported in part by funding to YLW from NIH (R21-EB023507, R21-NS121706, R21-NS142555), AHA (18CDA34140024), and DoD (W81XWH1810070, W81XWH-22-1-0221).

Conflicts of Interest: The authors declare no conflicts of interest.

References

1. Olson HE, Demarest ST, Pestana-Knight EM, Swanson LC, Iqbal S, Lal D, Leonard H, Cross JH, Devinsky O, Benke TA. Cyclin-Dependent Kinase-Like 5 Deficiency Disorder: Clinical Review. *Pediatric neurology*. 2019;97:18-25. doi: 10.1016/j.pediatrneurol.2019.02.015
2. Bahi-Buisson N, Bienvenu T. CDKL5-Related Disorders: From Clinical Description to Molecular Genetics. *Mol Syndromol*. 2012;2:137-152. doi: 10.1159/000331333
3. Demarest ST, Olson HE, Moss A, Pestana-Knight E, Zhang X, Parikh S, Swanson LC, Riley KD, Bazin GA, Angione K, et al. CDKL5 deficiency disorder: Relationship between genotype, epilepsy, cortical visual impairment, and development. *Epilepsia*. 2019;60:1733-1742. doi: 10.1111/epi.16285

4. Jakimiec M, Paprocka J, Śmigiel R. CDKL5 Deficiency Disorder-A Complex Epileptic Encephalopathy. *Brain Sci.* 2020;10. doi: 10.3390/brainsci10020107
5. Montini E, Andolfi G, Caruso A, Buchner G, Walpole SM, Mariani M, Consalez G, Trump D, Ballabio A, Franco B. Identification and characterization of a novel serine-threonine kinase gene from the Xp22 region. *Genomics.* 1998;51:427-433. doi: 10.1006/geno.1998.5391
6. Kalscheuer VM, Tao J, Donnelly A, Hollway G, Schwinger E, Kübart S, Menzel C, Hoeltzenbein M, Tommerup N, Eyre H, et al. Disruption of the serine/threonine kinase 9 gene causes severe X-linked infantile spasms and mental retardation. *Am J Hum Genet.* 2003;72:1401-1411. doi: 10.1086/375538
7. Fichou Y, Nectoux J, Bahi-Buisson N, Chelly J, Bienvenu T. An isoform of the severe encephalopathy-related CDKL5 gene, including a novel exon with extremely high sequence conservation, is specifically expressed in brain. *J Hum Genet.* 2011;56:52-57. doi: 10.1038/jhg.2010.143
8. Rademacher N, Hambrock M, Fischer U, Moser B, Ceulemans B, Lieb W, Boor R, Stefanova I, Gillissen-Kaesbach G, Runge C, et al. Identification of a novel CDKL5 exon and pathogenic mutations in patients with severe mental retardation, early-onset seizures and Rett-like features. *Neurogenetics.* 2011;12:165-167. doi: 10.1007/s10048-011-0277-6
9. Williamson SL, Giudici L, Kilstrup-Nielsen C, Gold W, Pelka GJ, Tam PP, Grimm A, Prodi D, Landsberger N, Christodoulou J. A novel transcript of cyclin-dependent kinase-like 5 (CDKL5) has an alternative C-terminus and is the predominant transcript in brain. *Hum Genet.* 2012;131:187-200. doi: 10.1007/s00439-011-1058-x
10. Leonard H, Downs J, Benke TA, Swanson L, Olson H, Demarest S. CDKL5 deficiency disorder: clinical features, diagnosis, and management. *The Lancet Neurology.* 2022;21:563-576. doi: 10.1016/s1474-4422(22)00035-7
11. Bahi-Buisson N, Nectoux J, Rosas-Vargas H, Milh M, Boddaert N, Girard B, Cances C, Ville D, Afenjar A, Rio M, et al. Key clinical features to identify girls with CDKL5 mutations. *Brain.* 2008;131:2647-2661. doi: 10.1093/brain/awn197
12. Sampedro-Castañeda M, Baltussen LL, Lopes AT, Qiu Y, Sirvio L, Mihaylov SR, Claxton S, Richardson JC, Lignani G, Ultanir SK. Epilepsy-linked kinase CDKL5 phosphorylates voltage-gated calcium channel Cav2.3, altering inactivation kinetics and neuronal excitability. *Nature Communications.* 2023;14:7830. doi: 10.1038/s41467-023-43475-w
13. Kadam SD, Sullivan BJ, Goyal A, Blue ME, Smith-Hicks C. Rett Syndrome and CDKL5 Deficiency Disorder: From Bench to Clinic. *International journal of molecular sciences.* 2019;20. doi: 10.3390/ijms20205098
14. Laurvick CL, de Klerk N, Bower C, Christodoulou J, Ravine D, Ellaway C, Williamson S, Leonard H. Rett syndrome in Australia: a review of the epidemiology. *The Journal of pediatrics.* 2006;148:347-352. doi: 10.1016/j.jpeds.2005.10.037
15. Artuso R, Mencarelli MA, Polli R, Sartori S, Ariani F, Pollazzon M, Marozza A, Cilio MR, Specchio N, Vigeveno F, et al. Early-onset seizure variant of Rett syndrome: definition of the clinical diagnostic criteria. *Brain Dev.* 2010;32:17-24. doi: 10.1016/j.braindev.2009.02.004
16. Silvestre M, Dempster K, Mihaylov SR, Claxton S, Ultanir SK. Cell type-specific expression, regulation and compensation of CDKL5 activity in mouse brain. *Mol Psychiatry.* 2024;29:1844-1856. doi: 10.1038/s41380-024-02434-7
17. Vossler D, Gidal B, Committee AT. A Summary of Antiseizure Medications Available in the United States: 4th Edition. American Epilepsy Society. 2024. Accessed April 1, 2024.
18. Olson HE, Daniels CI, Haviland I, Swanson LC, Greene CA, Denny AMM, Demarest ST, Pestana-Knight E, Zhang X, Moosa AN, et al. Current neurologic treatment and emerging therapies in CDKL5 deficiency disorder. *J Neurodev Disord.* 2021;13:40. doi: 10.1186/s11689-021-09384-z
19. Dell'Isola GB, Portwood KE, Consing K, Fattorusso A, Bartocci A, Ferrara P, Di Cara G, Verrotti A, Lodolo M. Current Overview of CDKL-5 Deficiency Disorder Treatment. *Pediatr Rep.* 2024;16:21-25. doi: 10.3390/pediatric16010002
20. FDA UFaDA. FDA approves drug for treatment of seizures associated with rare disease in patients two years of age and older, <https://www.fda.gov/drugs/news-events-human-drugs/fda-approves-drug-treatment-seizures-associated-rare-disease-patients-two-years-age-and-older>. 2022.

21. Junaid M, Wong K, Korolainen MA, Amin S, Downs J, Leonard H. Measuring the Burden of Epilepsy Hospitalizations in CDKL5 Deficiency Disorder. *Pediatric neurology*. 2025;163:68-75. doi: 10.1016/j.pediatrneurol.2024.11.010
22. Lavery D, Cronin A, Rakibuz-Zaman M, Crosby K, Gwadry - Sridhar F. PCR70 Diagnostic Journey, Seizure Burden, and Quality of Life Among Patients With CDKL5 Deficiency Disorder Using Real-World Data. *Value in Health*. 2024;27:S308. doi: 10.1016/j.jval.2024.03.1949
23. Wong K, Junaid M, Alexander S, Olson HE, Pestana-Knight EM, Rajaraman RR, Downs J, Leonard H. Caregiver Perspective of Benefits and Side Effects of Anti-Seizure Medications in CDKL5 Deficiency Disorder from an International Database. *CNS drugs*. 2024;38:719-732. doi: 10.1007/s40263-024-01105-z
24. Velarde-García JF, Güeita-Rodríguez J, Jiménez-Antona C, García-Bravo C, Aledo-Serrano Á, Gómez-Sánchez SM, Palacios-Ceña D. The impact of developmental and epileptic encephalopathies on families: a qualitative study. *Eur J Pediatr*. 2024;183:4103-4110. doi: 10.1007/s00431-024-05677-2
25. Amin S, Møller RS, Aledo-Serrano A, Arzimanoglou A, Bager P, Józwiak S, Kluger GJ, López-Cabeza S, Nabbout R, Partridge CA, et al. Providing quality care for people with CDKL5 deficiency disorder: A European expert panel opinion on the patient journey. *Epilepsia open*. 2024;9:832-849. doi: 10.1002/epi4.12914
26. Gautam N. Grant from the California Institute for Regenerative Medicine will fund research into CDKL5. UC Davis MIND Institute. 2022. Accessed August 10, 2022.
27. Jogani J, Stansfield N. CDKL5 and Gene Therapy. Strategic Alliance Partnership. 2025. Accessed September 24, 2025.
28. Medici G, Tassinari M, Loi M, Bove AM, Casadei Garofani B, Volpedo G, Mottolose N, Matteoli G, Lo Martire V, Berteotti C, et al. Safety and efficacy of Igk-TATk-CDKL5 gene therapy in mosaic CDKL5 deficiency. *Neurotherapeutics : the journal of the American Society for Experimental Neurotherapeutics*. 2025:e00727. doi: 10.1016/j.neurot.2025.e00727
29. Song X, Xia Z, Martinez D, Xu B, Spritzer Z, Zhang Y, Nugent E, Ho Y, Terzic B, Zhou Z. Independent genetic strategies define the scope and limits of CDKL5 deficiency disorder reversal. *Cell Rep Med*. 2025;6:101926. doi: 10.1016/j.xcrm.2024.101926
30. Ultragenyx. UX055 AAV9 gene therapy for the potential treatment of CDKL5 Deficiency Disorder (CDD). 2025.
31. Voronin G, Narasimhan J, Gittens J, Sheedy J, Lipari P, Peters M, DeMarco S, Cao L, Varganov Y, Kim MJ, et al. Preclinical studies of gene replacement therapy for CDKL5 deficiency disorder. *Mol Ther*. 2024;32:3331-3345. doi: 10.1016/j.ymthe.2024.07.012
32. Vázquez-Montante JJ, Márquez-Rojo P, Saavedra-Milán B, Hernández-Medrano C, Bravo-Oro A. Clinical and molecular heterogeneity in CDKL5 disorders. *Bol Med Hosp Infant Mex*. 2023;80:47-52. doi: 10.24875/bmhim.22000100
33. Disorders NNOoR. CDKL5 Deficiency Disorder. NORD National Organization of Rare Disorders. 2024. Accessed 4/25/2024.
34. Wang IT, Allen M, Goffin D, Zhu X, Fairless AH, Brodtkin ES, Siegel SJ, Marsh ED, Blendy JA, Zhou Z. Loss of CDKL5 disrupts kinome profile and event-related potentials leading to autistic-like phenotypes in mice. *Proceedings of the National Academy of Sciences of the United States of America*. 2012;109:21516-21521. doi: 10.1073/pnas.1216988110
35. Tang S, Terzic B, Wang IJ, Sarmiento N, Sizov K, Cui Y, Takano H, Marsh ED, Zhou Z, Coulter DA. Altered NMDAR signaling underlies autistic-like features in mouse models of CDKL5 deficiency disorder. *Nat Commun*. 2019;10:2655. doi: 10.1038/s41467-019-10689-w
36. Okuda K, Takao K, Watanabe A, Miyakawa T, Mizuguchi M, Tanaka T. Comprehensive behavioral analysis of the Cdkl5 knockout mice revealed significant enhancement in anxiety- and fear-related behaviors and impairment in both acquisition and long-term retention of spatial reference memory. *PLoS one*. 2018;13:e0196587. doi: 10.1371/journal.pone.0196587
37. Amendola E, Zhan Y, Mattucci C, Castroflorio E, Calcagno E, Fuchs C, Lonetti G, Silingardi D, Vyssotski AL, Farley D, et al. Mapping pathological phenotypes in a mouse model of CDKL5 disorder. *PLoS one*. 2014;9:e91613. doi: 10.1371/journal.pone.0091613

38. Mari F, Azimonti S, Bertani I, Bolognese F, Colombo E, Caselli R, Scala E, Longo I, Grosso S, Pescucci C, et al. CDKL5 belongs to the same molecular pathway of MeCP2 and it is responsible for the early-onset seizure variant of Rett syndrome. *Human molecular genetics*. 2005;14:1935-1946. doi: 10.1093/hmg/ddi198
39. Tang S, Wang IJ, Yue C, Takano H, Terzic B, Pance K, Lee JY, Cui Y, Coulter DA, Zhou Z. Loss of CDKL5 in Glutamatergic Neurons Disrupts Hippocampal Microcircuitry and Leads to Memory Impairment in Mice. *J Neurosci*. 2017;37:7420-7437. doi: 10.1523/jneurosci.0539-17.2017
40. Mulcahey PJ, Tang S, Takano H, White A, Davila Portillo DR, Kane OM, Marsh ED, Zhou Z, Coulter DA. Aged heterozygous Cdkl5 mutant mice exhibit spontaneous epileptic spasms. *Exp Neurol*. 2020;332:113388. doi: 10.1016/j.expneurol.2020.113388
41. Gennaccaro L, Fuchs C, Loi M, Pizzo R, Alvente S, Berteotti C, Lupori L, Sagona G, Galvani G, Gurgone A, et al. Age-Related Cognitive and Motor Decline in a Mouse Model of CDKL5 Deficiency Disorder is Associated with Increased Neuronal Senescence and Death. *Aging Dis*. 2021;12:764-785. doi: 10.14336/ad.2020.0827
42. Fuchs C, Gennaccaro L, Trazzi S, Bastianini S, Bettini S, Lo Martire V, Ren E, Medici G, Zoccoli G, Rimondini R, et al. Heterozygous CDKL5 Knockout Female Mice Are a Valuable Animal Model for CDKL5 Disorder. *Neural plasticity*. 2018;2018:9726950. doi: 10.1155/2018/9726950
43. Purtell H, Dhamne SC, Gurnani S, Bainbridge E, Modi ME, Lammers SHT, Super CE, Hameed MQ, Johnson EL, 3rd, Sahin M, et al. Electrographic spikes are common in wildtype mice. *Epilepsy & behavior : E&B*. 2018;89:94-98. doi: 10.1016/j.yebeh.2018.09.003
44. Basser PJ, Pierpaoli C. Microstructural and physiological features of tissues elucidated by quantitative-diffusion-tensor MRI. *J Magn Reson B*. 1996;111:209-219.
45. Basser PJ, Mattiello J, LeBihan D. Estimation of the effective self-diffusion tensor from the NMR spin echo. *J Magn Reson B*. 1994;103:247-254.
46. Basser PJ, Pajevic S, Pierpaoli C, Duda J, Aldroubi A. In vivo fiber tractography using DT-MRI data. *Magnetic resonance in medicine*. 2000;44:625-632. doi: 10.1002/1522-2594(200010)44:4<625::AID-MRM17>3.0.CO;2-O [pii]
47. Pierpaoli C, Basser PJ. Toward a quantitative assessment of diffusion anisotropy. *Magnetic resonance in medicine*. 1996;36:893-906.
48. Pierpaoli C, Jezzard P, Basser PJ, Barnett A, Di Chiro G. Diffusion tensor MR imaging of the human brain. *Radiology*. 1996;201:637-648.
49. Mori S, van Zijl PC. Diffusion weighting by the trace of the diffusion tensor within a single scan. *Magnetic resonance in medicine*. 1995;33:41-52. doi: 10.1002/mrm.1910330107
50. Mori S, Crain BJ, Chacko VP, van Zijl PC. Three-dimensional tracking of axonal projections in the brain by magnetic resonance imaging. *Ann Neurol*. 1999;45:265-269.
51. Xue R, van Zijl PC, Crain BJ, Solaiyappan M, Mori S. In vivo three-dimensional reconstruction of rat brain axonal projections by diffusion tensor imaging. *Magnetic resonance in medicine*. 1999;42:1123-1127. doi: 10.1002/(sici)1522-2594(199912)42:6<1123::aid-mrm17>3.0.co;2-h
52. Mori S, Itoh R, Zhang J, Kaufmann WE, van Zijl PC, Solaiyappan M, Yarowsky P. Diffusion tensor imaging of the developing mouse brain. *Magnetic resonance in medicine*. 2001;46:18-23. doi: 10.1002/mrm.1155
53. O'Donnell LJ, Westin CF. An introduction to diffusion tensor image analysis. *Neurosurg Clin N Am*. 2011;22:185-196, viii. doi: 10.1016/j.nec.2010.12.004
54. Ackerman JJH, Neil JJ. Biophysics of Diffusion in Cells. In: Jones DK, ed. *Diffusion MRI: Theory, Methods and Applications*. Oxford U. Press, Oxford; 2010:110-124.
55. Beaulieu C. The basis of anisotropic water diffusion in the nervous system - a technical review. *NMR in biomedicine*. 2002;15:435-455. doi: 10.1002/nbm.782
56. Le Bihan D, Turner R, Douek P. Is water diffusion restricted in human brain white matter? An echo-planar NMR imaging study. *Neuroreport*. 1993;4:887-890. doi: 10.1097/00001756-199307000-00012
57. Norris DG. The effects of microscopic tissue parameters on the diffusion weighted magnetic resonance imaging experiment. *NMR in biomedicine*. 2001;14:77-93. doi: 10.1002/nbm.682
58. Tuch DS, Reese TG, Wiegell MR, Van JW. Diffusion MRI of Complex Neural Architecture. *Neuron*. 2003;40:885-895. doi: https://doi.org/10.1016/S0896-6273(03)00758-X

59. Alexander DC, Barker GJ. Optimal imaging parameters for fiber-orientation estimation in diffusion MRI. *NeuroImage*. 2005;27:357-367. doi: S1053-8119(05)00268-5 [pii] 10.1016/j.neuroimage.2005.04.008
60. Wiegell MR, Larsson HB, Wedeen VJ. Fiber crossing in human brain depicted with diffusion tensor MR imaging. *Radiology*. 2000;217:897-903.
61. Vos SB, Jones DK, Jeurissen B, Viergever MA, Leemans A. The influence of complex white matter architecture on the mean diffusivity in diffusion tensor MRI of the human brain. *NeuroImage*. 2012;59:2208-2216. doi: S1053-8119(11)01162-1 [pii] 10.1016/j.neuroimage.2011.09.086
62. Tuch DS, Reese TG, Wiegell MR, Makris N, Belliveau JW, Wedeen VJ. High angular resolution diffusion imaging reveals intravoxel white matter fiber heterogeneity. *Magnetic resonance in medicine*. 2002;48:577-582. doi: 10.1002/mrm.10268
63. Alexander AL, Hasan KM, Lazar M, Tsuruda JS, Parker DL. Analysis of partial volume effects in diffusion-tensor MRI. *Magnetic resonance in medicine*. 2001;45:770-780. doi: 10.1002/mrm.1105 [pii]
64. Wang Q, Ding SL, Li Y, Royall J, Feng D, Lesnar P, Graddis N, Naeemi M, Facer B, Ho A, et al. The Allen Mouse Brain Common Coordinate Framework: A 3D Reference Atlas. *Cell*. 2020;181:936-953.e920. doi: 10.1016/j.cell.2020.04.007
65. MacKenzie-Graham A, Jones ES, Shattuck DW, Dinov ID, Bota M, Toga AW. The informatics of a C57BL/6J mouse brain atlas. *Neuroinformatics*. 2003;1:397-410. doi: 10.1385/ni:1:4:397
66. Science AIfB. Allen Mouse Brain Atlas <https://mouse.brain-map.org/static/atlas>. 2020.
67. Stapleton MC, Koch SP, Cortes DRE, Wyman S, Schwab KE, Mueller S, McKennan CG, Boehm-Sturm P, Wu YL. Apolipoprotein-E deficiency leads to brain network alteration characterized by diffusion MRI and graph theory. *Frontiers in neuroscience*. 2023;17:1183312. doi: 10.3389/fnins.2023.1183312
68. Ashburner J, Friston KJ. Unified segmentation. *NeuroImage*. 2005;26:839-851. doi: 10.1016/j.neuroimage.2005.02.018
69. Friston KJ, Holmes AP, Worsley KJ, Poline J-P, Frith CD, Frackowiak RSJ. Statistical parametric maps in functional imaging: A general linear approach. *Human Brain Mapping*. 1994;2:189-210. doi: <https://doi.org/10.1002/hbm.460020402>
70. Hikishima K, Komaki Y, Seki F, Ohnishi Y, Okano HJ, Okano H. In vivo microscopic voxel-based morphometry with a brain template to characterize strain-specific structures in the mouse brain. *Sci Rep*. 2017;7:85. doi: 10.1038/s41598-017-00148-1
71. Klein S, Staring M, Murphy K, Viergever MA, Pluim JP. elastix: a toolbox for intensity-based medical image registration. *IEEE Trans Med Imaging*. 2010;29:196-205. doi: 10.1109/tmi.2009.2035616
72. Scharwächter L, Schmitt FJ, Pallast N, Fink GR, Aswendt M. Network analysis of neuroimaging in mice. *NeuroImage*. 2022;253:119110. doi: <https://doi.org/10.1016/j.neuroimage.2022.119110>
73. Ingalhalikar M, Parker D, Ghanbari Y, Smith A, Hua K, Mori S, Abel T, Davatzikos C, Verma R. Connectome and Maturation Profiles of the Developing Mouse Brain Using Diffusion Tensor Imaging. *Cerebral cortex (New York, NY : 1991)*. 2015;25:2696-2706. doi: 10.1093/cercor/bhu068
74. Rubinov M, Sporns O. Complex network measures of brain connectivity: uses and interpretations. *NeuroImage*. 2010;52:1059-1069. doi: 10.1016/j.neuroimage.2009.10.003
75. Bullmore E, Sporns O. Complex brain networks: graph theoretical analysis of structural and functional systems. *Nat Rev Neurosci*. 2009;10:186-198. doi: 10.1038/nrn2575
76. Benjamini Y, Hochberg Y. Controlling the False Discovery Rate: A Practical and Powerful Approach to Multiple Testing. *Journal of the Royal Statistical Society Series B (Methodological)*. 1995;57:289-300.
77. Landman BA, Wan H, Bogovic JA, Bazin PL, Prince JL. Resolution of Crossing Fibers with Constrained Compressed Sensing using Traditional Diffusion Tensor MRI. *Proc SPIE Int Soc Opt Eng*. 2010;7623:76231h. doi: 10.1117/12.844171
78. Wong HH, Chou CYC, Watt AJ, Sjöström PJ. Comparing mouse and human brains. *Elife*. 2023;12. doi: 10.7554/eLife.90017
79. Sun T, Hevner RF. Growth and folding of the mammalian cerebral cortex: from molecules to malformations. *Nat Rev Neurosci*. 2014;15:217-232. doi: 10.1038/nrn3707

80. Xu N, LaGrow TJ, Anumba N, Lee A, Zhang X, Yousefi B, Bassil Y, Clavijo GP, Khalilzad Sharghi V, Maltbie E, et al. Functional Connectivity of the Brain Across Rodents and Humans. *Frontiers in neuroscience*. 2022;16:816331. doi: 10.3389/fnins.2022.816331
81. Li C, Li J, Lai L, Li S, Yan S. Genetically engineered pig models of neurological diseases. *Ageing and Neurodegenerative Diseases*. 2022;2:13. doi: 10.20517/and.2022.13
82. Kjer HM, Andersson M, He Y, Pacureanu A, Daducci A, Pizzolato M, Salditt T, Robisch A-L, Eckermann M, Töpperwien M, et al. Bridging the 3D geometrical organisation of white matter pathways across anatomical length scales and species. *eLife*. 2025;13:RP94917. doi: 10.7554/eLife.94917
83. Zhang J. Diffusion tensor imaging of white matter pathology in the mouse brain. *Imaging Med*. 2010;2:623-632. doi: 10.2217/iim.10.60
84. Müller HP, Roselli F, Rasche V, Kassubek J. Diffusion Tensor Imaging-Based Studies at the Group-Level Applied to Animal Models of Neurodegenerative Diseases. *Frontiers in neuroscience*. 2020;14:734. doi: 10.3389/fnins.2020.00734
85. Abhinav K, Yeh FC, Mansouri A, Zadeh G, Fernandez-Miranda JC. High-definition fiber tractography for the evaluation of perilesional white matter tracts in high-grade glioma surgery. *Neuro Oncol*. 2015;17:1199-1209. doi: 10.1093/neuonc/nov113
86. Yeh FC, Wedeen VJ, Tseng WY. Generalized q-sampling imaging. *IEEE Trans Med Imaging*. 2010;29:1626-1635. doi: 10.1109/TMI.2010.2045126
87. Yeh FC, Verstynen TD, Wang Y, Fernandez-Miranda JC, Tseng WY. Deterministic diffusion fiber tracking improved by quantitative anisotropy. *PloS one*. 2013;8:e80713. doi: 10.1371/journal.pone.0080713. PONE-D-13-26801 [pii]
88. Conturo TE, Lori NF, Cull TS, Akbudak E, Snyder AZ, Shimony JS, McKinstry RC, Burton H, Raichle ME. Tracking neuronal fiber pathways in the living human brain. *Proceedings of the National Academy of Sciences of the United States of America*. 1999;96:10422-10427.
89. Shen CY, Tyan YS, Kuo LW, Wu CW, Weng JC. Quantitative Evaluation of Rabbit Brain Injury after Cerebral Hemisphere Radiation Exposure Using Generalized q-Sampling Imaging. *PloS one*. 2015;10:e0133001. doi: 10.1371/journal.pone.0133001
90. Lim SY, Tyan YS, Chao YP, Nien FY, Weng JC. New insights into the developing rabbit brain using diffusion tensor tractography and generalized q-sampling MRI. *PloS one*. 2015;10:e0119932. doi: 10.1371/journal.pone.0119932
91. Zhang H, Wang Y, Lu T, Qiu B, Tang Y, Ou S, Tie X, Sun C, Xu K, Wang Y. Differences between generalized q-sampling imaging and diffusion tensor imaging in the preoperative visualization of the nerve fiber tracts within peritumoral edema in brain. *Neurosurgery*. 2013;73:1044-1053; discussion 1053. doi: 10.1227/NEU.0000000000000146
92. Yeh FC, Tseng WY. Sparse solution of fiber orientation distribution function by diffusion decomposition. *PloS one*. 2013;8:e75747. doi: 10.1371/journal.pone.0075747. PONE-D-13-11252 [pii]
93. Yeh FC, Wedeen VJ, Tseng WY. Estimation of fiber orientation and spin density distribution by diffusion deconvolution. *NeuroImage*. 2011;55:1054-1062. doi: 10.1016/j.neuroimage.2010.11.087
94. Berman JI, Lanza MR, Blaskey L, Edgar JC, Roberts TP. High angular resolution diffusion imaging probabilistic tractography of the auditory radiation. *AJNR American journal of neuroradiology*. 2013;34:1573-1578. doi: 10.3174/ajnr.A3471
95. Caiazzo G, Fratello M, Di Nardo F, Trojsi F, Tedeschi G, Esposito F. Structural connectome with high angular resolution diffusion imaging MRI: assessing the impact of diffusion weighting and sampling on graph-theoretic measures. *Neuroradiology*. 2018;60:497-504. doi: 10.1007/s00234-018-2003-7
96. Tong Q, He H, Gong T, Li C, Liang P, Qian T, Sun Y, Ding Q, Li K, Zhong J. Multicenter dataset of multi-shell diffusion MRI in healthy traveling adults with identical settings. *Scientific Data*. 2020;7:157. doi: 10.1038/s41597-020-0493-8
97. Li CX, Patel S, Zhang X. Evaluation of multi-shell diffusion MRI acquisition strategy on quantitative analysis using multi-compartment models. *Quant Imaging Med Surg*. 2020;10:824-834. doi: 10.21037/qims.2020.03.11

98. Vanden Bulcke C, Stölting A, Maric D, Macq B, Absinta M, Maggi P. Comparative overview of multi-shell diffusion MRI models to characterize the microstructure of multiple sclerosis lesions and periplaques. *NeuroImage: Clinical*. 2024;42:103593. doi: <https://doi.org/10.1016/j.nicl.2024.103593>
99. Descoteaux M, Deriche R, Knosche TR, Anwander A. Deterministic and probabilistic tractography based on complex fibre orientation distributions. *IEEE Trans Med Imaging*. 2009;28:269-286. doi: 10.1109/TMI.2008.2004424
100. Wedeen VJ, Wang RP, Schmahmann JD, Benner T, Tseng WY, Dai G, Pandya DN, Hagmann P, D'Arceuil H, de Crespigny AJ. Diffusion spectrum magnetic resonance imaging (DSI) tractography of crossing fibers. *NeuroImage*. 2008;41:1267-1277. doi: S1053-8119(08)00253-X [pii] 10.1016/j.neuroimage.2008.03.036
101. Mori S, Barker PB. Diffusion magnetic resonance imaging: its principle and applications. *Anat Rec*. 1999;257:102-109. doi: 10.1002/(sici)1097-0185(19990615)257:3<102::Aid-ar7>3.0.Co;2-6
102. Winklewski PJ, Sabisz A, Naumczyk P, Jodzio K, Szurowska E, Szarmach A. Understanding the Physiopathology Behind Axial and Radial Diffusivity Changes-What Do We Know? *Front Neurol*. 2018;9:92. doi: 10.3389/fneur.2018.00092
103. Wheeler-Kingshott CA, Cercignani M. About "axial" and "radial" diffusivities. *Magnetic resonance in medicine*. 2009;61:1255-1260. doi: 10.1002/mrm.21965
104. Sun SW, Liang HF, Trinkaus K, Cross AH, Armstrong RC, Song SK. Noninvasive detection of cuprizone induced axonal damage and demyelination in the mouse corpus callosum. *Magnetic resonance in medicine*. 2006;55:302-308. doi: 10.1002/mrm.20774
105. Budde MD, Xie M, Cross AH, Song SK. Axial diffusivity is the primary correlate of axonal injury in the experimental autoimmune encephalomyelitis spinal cord: a quantitative pixelwise analysis. *J Neurosci*. 2009;29:2805-2813. doi: 29/9/2805 [pii] 10.1523/JNEUROSCI.4605-08.2009
106. Song SK, Sun SW, Ramsbottom MJ, Chang C, Russell J, Cross AH. Dysmyelination revealed through MRI as increased radial (but unchanged axial) diffusion of water. *NeuroImage*. 2002;17:1429-1436. doi: S105381190291267X [pii]
107. Song SK, Yoshino J, Le TQ, Lin SJ, Sun SW, Cross AH, Armstrong RC. Demyelination increases radial diffusivity in corpus callosum of mouse brain. *NeuroImage*. 2005;26:132-140. doi: S1053-8119(05)00022-4 [pii] 10.1016/j.neuroimage.2005.01.028
108. Kumar R, Nguyen HD, Macey PM, Woo MA, Harper RM. Regional brain axial and radial diffusivity changes during development. *Journal of neuroscience research*. 2012;90:346-355. doi: 10.1002/jnr.22757
109. Barnea-Goraly N, Menon V, Eckert M, Tamm L, Bammner R, Karchemskiy A, Dant CC, Reiss AL. White matter development during childhood and adolescence: a cross-sectional diffusion tensor imaging study. *Cerebral cortex (New York, NY : 1991)*. 2005;15:1848-1854. doi: 10.1093/cercor/bhi062
110. Mukherjee P, Miller JH, Shimony JS, Philip JV, Nehra D, Snyder AZ, Conturo TE, Neil JJ, McKinstry RC. Diffusion-tensor MR imaging of gray and white matter development during normal human brain maturation. *AJNR American journal of neuroradiology*. 2002;23:1445-1456.
111. Counsell SJ, Shen Y, Boardman JP, Larkman DJ, Kapellou O, Ward P, Allsop JM, Cowan FM, Hajnal JV, Edwards AD, et al. Axial and radial diffusivity in preterm infants who have diffuse white matter changes on magnetic resonance imaging at term-equivalent age. *Pediatrics*. 2006;117:376-386. doi: 10.1542/peds.2005-0820
112. Quinones JF, Hildebrandt A, Pavan T, Thiel CM, Heep A. Preterm birth and neonatal white matter microstructure in in-vivo reconstructed fiber tracts among audiovisual integration brain regions. *Developmental Cognitive Neuroscience*. 2023;60:101202. doi: <https://doi.org/10.1016/j.dcn.2023.101202>
113. Dibble M, Ang JZ, Mariga L, Molloy EJ, Bokde ALW. Diffusion Tensor Imaging in Very Preterm, Moderate-Late Preterm and Term-Born Neonates: A Systematic Review. *The Journal of pediatrics*. 2021;232:48-58.e43. doi: 10.1016/j.jpeds.2021.01.008
114. Rogers CE, Smyser T, Smyser CD, Shimony J, Inder TE, Neil JJ. Regional white matter development in very preterm infants: perinatal predictors and early developmental outcomes. *Pediatric research*. 2016;79:87-95. doi: 10.1038/pr.2015.172

115. Vandermosten M, Boets B, Wouters J, Ghesquière P. A qualitative and quantitative review of diffusion tensor imaging studies in reading and dyslexia. *Neuroscience and biobehavioral reviews*. 2012;36:1532-1552. doi: 10.1016/j.neubiorev.2012.04.002
116. Vandermosten M, Boets B, Poelmans H, Sunaert S, Wouters J, Ghesquière P. A tractography study in dyslexia: neuroanatomic correlates of orthographic, phonological and speech processing. *Brain*. 2012;135:935-948. doi: 10.1093/brain/awr363
117. El-Sady S, Mohammad SA, Aboualfotouh Ahmed K, Khattab AN, Nashaat NH, Orabi G, Abdelraouf ER. Correlation between diffusion tensor imaging measures and the reading and cognitive performance of Arabic readers: dyslexic children perspective. *Neuroradiology*. 2020;62:525-531. doi: 10.1007/s00234-020-02368-1
118. Mac Donald CL, Johnson AM, Cooper D, Nelson EC, Werner NJ, Shimony JS, Snyder AZ, Raichle ME, Witherow JR, Fang R, et al. Detection of blast-related traumatic brain injury in U.S. military personnel. *The New England journal of medicine*. 2011;364:2091-2100. doi: 10.1056/NEJMoa1008069
119. Aung WY, Mar S, Benzinger TL. Diffusion tensor MRI as a biomarker in axonal and myelin damage. *Imaging Med*. 2013;5:427-440. doi: 10.2217/iim.13.49
120. Arfanakis K, Houghton VM, Carew JD, Rogers BP, Dempsey RJ, Meyerand ME. Diffusion tensor MR imaging in diffuse axonal injury. *AJNR American journal of neuroradiology*. 2002;23:794-802.
121. Robinson S, Berglass JB, Denson JL, Berkner J, Anstine CV, Winer JL, Maxwell JR, Qiu J, Yang Y, Sillerud LO, et al. Microstructural and microglial changes after repetitive mild traumatic brain injury in mice. *Journal of neuroscience research*. 2017;95:1025-1035. doi: 10.1002/jnr.23848
122. Bennett RE, Mac Donald CL, Brody DL. Diffusion tensor imaging detects axonal injury in a mouse model of repetitive closed-skull traumatic brain injury. *Neuroscience letters*. 2012;513:160-165. doi: 10.1016/j.neulet.2012.02.024
123. Du G, Lewis MM, Kanekar S, Sterling NW, He L, Kong L, Li R, Huang X. Combined Diffusion Tensor Imaging and Apparent Transverse Relaxation Rate Differentiate Parkinson Disease and Atypical Parkinsonism. *AJNR American journal of neuroradiology*. 2017;38:966-972. doi: 10.3174/ajnr.A5136
124. Metwalli NS, Benatar M, Nair G, Usher S, Hu X, Carew JD. Utility of axial and radial diffusivity from diffusion tensor MRI as markers of neurodegeneration in amyotrophic lateral sclerosis. *Brain Res*. 2010;1348:156-164. doi: 10.1016/j.brainres.2010.05.067
125. Kamagata K, Andica C, Hatano T, Ogawa T, Takeshige-Amano H, Ogaki K, Akashi T, Hagiwara A, Fujita S, Aoki S. Advanced diffusion magnetic resonance imaging in patients with Alzheimer's and Parkinson's diseases. *Neural Regen Res*. 2020;15:1590-1600. doi: 10.4103/1673-5374.276326
126. Lin CP, Frigerio I, Bol J, Bouwman MMA, Wesseling AJ, Dahl MJ, Rozemuller AJM, van der Werf YD, Pouwels PJW, van de Berg WDJ, et al. Microstructural integrity of the locus coeruleus and its tracts reflect noradrenergic degeneration in Alzheimer's disease and Parkinson's disease. *Transl Neurodegener*. 2024;13:9. doi: 10.1186/s40035-024-00400-5
127. Naidu S, Kaufmann WE, Abrams MT, Pearlson GD, Lanham DC, Fredericksen KA, Barker PB, Horska A, Golay X, Mori S, et al. Neuroimaging studies in Rett syndrome. *Brain Dev*. 2001;23 Suppl 1:S62-71. doi: 10.1016/s0387-7604(01)00381-3
128. Awad PN, Zerbi V, Johnson-Venkatesh EM, Damiani F, Pagani M, Markicevic M, Nickles S, Gozzi A, Umemori H, Fagiolini M. CDKL5 sculpts functional callosal connectivity to promote cognitive flexibility. *Mol Psychiatry*. 2024;29:1698-1709. doi: 10.1038/s41380-023-01962-y
129. Olds J. Learning and the hippocampus. *Rev Can Biol*. 1972;31:Suppl:215-238.
130. McClelland JL, McNaughton BL, O'Reilly RC. Why there are complementary learning systems in the hippocampus and neocortex: insights from the successes and failures of connectionist models of learning and memory. *Psychol Rev*. 1995;102:419-457. doi: 10.1037/0033-295x.102.3.419
131. Biane JS, Ladow MA, Stefanini F, Boddu SP, Fan A, Hassan S, Dundar N, Apodaca-Montano DL, Zhou LZ, Fayner V, et al. Neural dynamics underlying associative learning in the dorsal and ventral hippocampus. *Nature neuroscience*. 2023;26:798-809. doi: 10.1038/s41593-023-01296-6
132. Dickerson KC, Delgado MR. Contributions of the hippocampus to feedback learning. *Cogn Affect Behav Neurosci*. 2015;15:861-877. doi: 10.3758/s13415-015-0364-5

133. Rogan MT, Staubli UV, LeDoux JE. Fear conditioning induces associative long-term potentiation in the amygdala. *Nature*. 1997;390:604-607. doi: 10.1038/37601
134. Dityatev AE, Bolshakov VY. Amygdala, long-term potentiation, and fear conditioning. *The Neuroscientist : a review journal bringing neurobiology, neurology and psychiatry*. 2005;11:75-88. doi: 10.1177/1073858404270857
135. Kochli DE, Thompson EC, Fricke EA, Postle AF, Quinn JJ. The amygdala is critical for trace, delay, and contextual fear conditioning. *Learning & memory (Cold Spring Harbor, NY)*. 2015;22:92-100. doi: 10.1101/lm.034918.114
136. Skelly MJ, Ariwodola OJ, Weiner JL. Fear conditioning selectively disrupts noradrenergic facilitation of GABAergic inhibition in the basolateral amygdala. *Neuropharmacology*. 2017;113:231-240. doi: 10.1016/j.neuropharm.2016.10.003
137. Kim WB, Cho JH. Encoding of Discriminative Fear Memory by Input-Specific LTP in the Amygdala. *Neuron*. 2017;95:1129-1146.e1125. doi: 10.1016/j.neuron.2017.08.004
138. Guillamón-Vivancos T, Favaloro F, Dori F, López-Bendito G. The superior colliculus: New insights into an evolutionarily ancient structure. *Current Opinion in Neurobiology*. 2024;89:102926. doi: https://doi.org/10.1016/j.conb.2024.102926
139. Ito S, Feldheim DA. The Mouse Superior Colliculus: An Emerging Model for Studying Circuit Formation and Function. *Front Neural Circuits*. 2018;12:10. doi: 10.3389/fncir.2018.00010
140. Goossens HH, van Opstal AJ. Optimal control of saccades by spatial-temporal activity patterns in the monkey superior colliculus. *PLoS Comput Biol*. 2012;8:e1002508. doi: 10.1371/journal.pcbi.1002508
141. Yuan P, Raz N. Prefrontal cortex and executive functions in healthy adults: a meta-analysis of structural neuroimaging studies. *Neuroscience and biobehavioral reviews*. 2014;42:180-192. doi: 10.1016/j.neubiorev.2014.02.005
142. Burzynska AZ, Nagel IE, Preuschhof C, Gluth S, Bäckman L, Li SC, Lindenberger U, Heekeren HR. Cortical thickness is linked to executive functioning in adulthood and aging. *Hum Brain Mapp*. 2012;33:1607-1620. doi: 10.1002/hbm.21311
143. Cao J, Xu J, Chen S, Fan F, Chen M, Liu F, Li G. Odor-mediated contextual learning induced memory consolidation and hippocampus development in neonate rat. *Neuroreport*. 2020;31:64-68. doi: 10.1097/wnr.0000000000001368
144. Yau SY, Li A, So KF. Involvement of Adult Hippocampal Neurogenesis in Learning and Forgetting. *Neural plasticity*. 2015;2015:717958. doi: 10.1155/2015/717958
145. Morris RG, Garrud P, Rawlins JN, O'Keefe J. Place navigation impaired in rats with hippocampal lesions. *Nature*. 1982;297:681-683.
146. Amsel A. Hippocampal function in the rat: cognitive mapping or vicarious trial and error? *Hippocampus*. 1993;3:251-256. doi: 10.1002/hipo.450030302
147. D'Hooge R, De Deyn PP. Applications of the Morris water maze in the study of learning and memory. *Brain research Brain research reviews*. 2001;36:60-90.
148. Wenk GL. Assessment of spatial memory using the radial arm maze and Morris water maze. *Current protocols in neuroscience*. 2004;Chapter 8:Unit 8.5A. doi: 10.1002/0471142301.ns0805as26
149. Sullivan EV, Rosenbloom MJ, Deshmukh A, Desmond JE, Pfefferbaum A. Alcohol and the Cerebellum: Effects on Balance, Motor Coordination, and Cognition. *Alcohol Health Res World*. 1995;19:138-141.
150. Kansal K, Yang Z, Fishman AM, Sair HI, Ying SH, Jedynek BM, Prince JL, Onyike CU. Structural cerebellar correlates of cognitive and motor dysfunctions in cerebellar degeneration. *Brain*. 2017;140:707-720. doi: 10.1093/brain/aww327
151. Johnson DM, Illig KR, Behan M, Haberly LB. New features of connectivity in piriform cortex visualized by intracellular injection of pyramidal cells suggest that "primary" olfactory cortex functions like "association" cortex in other sensory systems. *J Neurosci*. 2000;20:6974-6982. doi: 10.1523/jneurosci.20-18-06974.2000
152. Borghei A, Kelly R, Pearce JJ, Stoub TR, Sani S. Structural Connectivity of the Human Piriform Cortex: an Exploratory Study. *Neurosurgery*. 2024;94:856-863. doi: 10.1227/neu.0000000000002756
153. Miller WL. The Hypothalamic-Pituitary-Adrenal Axis: A Brief History. *Horm Res Paediatr*. 2018;89:212-223. doi: 10.1159/000487755

154. Fong H, Zheng J, Kurrasch D. The structural and functional complexity of the integrative hypothalamus. *Science*. 2023;382:388-394. doi: 10.1126/science.adh8488
155. Basso MA, May PJ. Circuits for Action and Cognition: A View from the Superior Colliculus. *Annu Rev Vis Sci*. 2017;3:197-226. doi: 10.1146/annurev-vision-102016-061234
156. Basso MA, Bickford ME, Cang J. Unraveling circuits of visual perception and cognition through the superior colliculus. *Neuron*. 2021;109:918-937. doi: 10.1016/j.neuron.2021.01.013
157. Ghitani N, Bayguinov PO, Basso MA, Jackson MB. A sodium afterdepolarization in rat superior colliculus neurons and its contribution to population activity. *J Neurophysiol*. 2016;116:191-200. doi: 10.1152/jn.01138.2015
158. Sporns O, Tononi G, Kötter R. The human connectome: A structural description of the human brain. *PLoS Comput Biol*. 2005;1:e42. doi: 10.1371/journal.pcbi.0010042
159. He Y, Evans A. Graph theoretical modeling of brain connectivity. *Current opinion in neurology*. 2010;23:341-350. doi: 10.1097/WCO.0b013e32833aa567
160. Bassett DS, Bullmore ET. Human brain networks in health and disease. *Current opinion in neurology*. 2009;22:340-347. doi: 10.1097/WCO.0b013e32832d93dd
161. Lo CY, He Y, Lin CP. Graph theoretical analysis of human brain structural networks. *Reviews in the neurosciences*. 2011;22:551-563. doi: 10.1515/rns.2011.039
162. Chiang S, Haneef Z. Graph theory findings in the pathophysiology of temporal lobe epilepsy. *Clinical neurophysiology : official journal of the International Federation of Clinical Neurophysiology*. 2014;125:1295-1305. doi: 10.1016/j.clinph.2014.04.004
163. Stam CJ, Reijneveld JC. Graph theoretical analysis of complex networks in the brain. *Nonlinear Biomedical Physics*. 2007;1:3. doi: 10.1186/1753-4631-1-3
164. Reijneveld JC, Ponten SC, Berendse HW, Stam CJ. The application of graph theoretical analysis to complex networks in the brain. *Clinical Neurophysiology*. 2007;118:2317-2331. doi: <https://doi.org/10.1016/j.clinph.2007.08.010>
165. Vecchio F, Miraglia F, Maria Rossini P. Connectome: Graph theory application in functional brain network architecture. *Clinical Neurophysiology Practice*. 2017;2:206-213. doi: <https://doi.org/10.1016/j.cnp.2017.09.003>
166. Rubinov M, Sporns O. Weight-conserving characterization of complex functional brain networks. *NeuroImage*. 2011;56:2068-2079. doi: 10.1016/j.neuroimage.2011.03.069
167. Cohen JR, D'Esposito M. The Segregation and Integration of Distinct Brain Networks and Their Relationship to Cognition. *J Neurosci*. 2016;36:12083-12094. doi: 10.1523/jneurosci.2965-15.2016
168. Bassett DS, Bullmore E. Small-world brain networks. *The Neuroscientist : a review journal bringing neurobiology, neurology and psychiatry*. 2006;12:512-523. doi: 10.1177/1073858406293182
169. Bassett DS, Bullmore ET. Small-World Brain Networks Revisited. *The Neuroscientist : a review journal bringing neurobiology, neurology and psychiatry*. 2017;23:499-516. doi: 10.1177/1073858416667720
170. Kukla B, Anthony M, Chen S, Turnbull A, Baran TM, Lin FV. Brain Small-Worldness Properties and Perceived Fatigue in Mild Cognitive Impairment. *J Gerontol A Biol Sci Med Sci*. 2022;77:541-546. doi: 10.1093/gerona/glab084
171. Medina JF, Repa JC, Mauk MD, LeDoux JE. Parallels between cerebellum- and amygdala-dependent conditioning. *Nat Rev Neurosci*. 2002;3:122-131. doi: 10.1038/nrn728
172. Téllez-Zenteno JF, Hernández-Ronquillo L. A review of the epidemiology of temporal lobe epilepsy. *Epilepsy Res Treat*. 2012;2012:630853. doi: 10.1155/2012/630853
173. Sinjab B, Martinian L, Sisodiya SM, Thom M. Regional thalamic neuropathology in patients with hippocampal sclerosis and epilepsy: a postmortem study. *Epilepsia*. 2013;54:2125-2133. doi: 10.1111/epi.12403
174. Feng L, Motelow JE, Ma C, Biche W, McCafferty C, Smith N, Liu M, Zhan Q, Jia R, Xiao B, et al. Seizures and Sleep in the Thalamus: Focal Limbic Seizures Show Divergent Activity Patterns in Different Thalamic Nuclei. *J Neurosci*. 2017;37:11441-11454. doi: 10.1523/jneurosci.1011-17.2017
175. Park KM, Kim TH, Mun CW, Shin KJ, Ha SY, Park J, Lee BI, Lee H-J, Kim SE. Reduction of ipsilateral thalamic volume in temporal lobe epilepsy with hippocampal sclerosis. *Journal of Clinical Neuroscience*. 2018;55:76-81. doi: <https://doi.org/10.1016/j.jocn.2018.06.025>

176. Cho KH, Lee HJ, Heo K, Kim SE, Lee DA, Park KM. Intrinsic Thalamic Network in Temporal Lobe Epilepsy With Hippocampal Sclerosis According to Surgical Outcomes.
177. Fisher RS. Deep brain stimulation of thalamus for epilepsy. *Neurobiology of disease*. 2023;179:106045. doi: <https://doi.org/10.1016/j.nbd.2023.106045>
178. Bouwens van der Vlis TAM, Schijns O, Schaper F, Hoogland G, Kubben P, Wagner L, Rouhl R, Temel Y, Ackermans L. Deep brain stimulation of the anterior nucleus of the thalamus for drug-resistant epilepsy. *Neurosurg Rev*. 2019;42:287-296. doi: 10.1007/s10143-017-0941-x
179. Shine JM, Lewis LD, Garrett DD, Hwang K. The impact of the human thalamus on brain-wide information processing. *Nature Reviews Neuroscience*. 2023;24:416-430. doi: 10.1038/s41583-023-00701-0
180. Marcuse LV, Langan M, Hof PR, Panov F, Saez I, Jimenez-Shahed J, Figeo M, Mayberg H, Yoo JY, Ghatan S, et al. The thalamus: Structure, function, and neurotherapeutics. *Neurotherapeutics : the journal of the American Society for Experimental NeuroTherapeutics*. 2025;22:e00550. doi: 10.1016/j.neurot.2025.e00550
181. Cacciatore M, Magnani FG, Barbadoro F, Ippoliti C, Stanziano M, Clementi L, Nigri A, Nanetti L, Marino S, La Porta F, et al. Thalamus and consciousness: a systematic review on thalamic nuclei associated with consciousness. *Front Neurol*. 2025;16:1509668. doi: 10.3389/fneur.2025.1509668
182. Specchio N, Trivisano M, Lenge M, Ferretti A, Mei D, Parrini E, Napolitano A, Rossi-Espagnet C, Talenti G, Longo D, et al. CDKL5 deficiency disorder: progressive brain atrophy may be part of the syndrome. *Cerebral cortex (New York, NY : 1991)*. 2023;33:9709-9717. doi: 10.1093/cercor/bhad235
183. Rodak M, Jonderko M, Rozwadowska P, Machnikowska-Sokołowska M, Paprocka J. CDKL5 Deficiency Disorder (CDD)—Rare Presentation in Male. *Children*. 2022;9. doi: 10.3390/children9121806
184. Takeguchi R, Akaba Y, Kuroda M, Tanaka R, Tanaka T, Itoh M, Takahashi S. Neurophysiological and brain structural insights into cyclin-dependent kinase-like 5 deficiency disorder: Visual and auditory evoked potentials and MRI analysis. *J Neurol Sci*. 2024;461:123063. doi: 10.1016/j.jns.2024.123063
185. Lupori L, Sagona G, Fuchs C, Mazziotti R, Stefanov A, Putignano E, Napoli D, Strettoi E, Ciani E, Pizzorusso T. Site-specific abnormalities in the visual system of a mouse model of CDKL5 deficiency disorder. *Human molecular genetics*. 2019;28:2851-2861. doi: 10.1093/hmg/ddz102
186. Carli S, Chaabane L, Butti C, De Palma C, Aimar P, Salio C, Vignoli A, Giustetto M, Landsberger N, Frasca A. In vivo magnetic resonance spectroscopy in the brain of Cdkl5 null mice reveals a metabolic profile indicative of mitochondrial dysfunctions. *J Neurochem*. 2021;157:1253-1269. doi: 10.1111/jnc.15300
187. Serrano RJ, Lee C, Douek AM, Kaslin J, Bryson-Richardson RJ, Sztal TE. Novel preclinical model for CDKL5 deficiency disorder. *Disease models & mechanisms*. 2022;15. doi: 10.1242/dmm.049094
188. Lupori L, Sagona G, Fuchs C, Mazziotti R, Stefanov A, Putignano E, Napoli D, Strettoi E, Ciani E, Pizzorusso T.
189. Benarroch E. What Are the Functions of the Superior Colliculus and Its Involvement in Neurologic Disorders? *Neurology*. 2023;100:784-790. doi: 10.1212/wnl.0000000000207254
190. Quintiliani M, Ricci D, Petrianni M, Leone S, Orazi L, Amore F, Gambardella ML, Contaldo I, Veredice C, Perulli M, et al. Cortical Visual Impairment in CDKL5 Deficiency Disorder. *Front Neurol*. 2021;12:805745. doi: 10.3389/fneur.2021.805745
191. Adhikari A, Buchanan FKB, Fenton TA, Cameron DL, Halmai J, Copping NA, Fink KD, Silverman JL. Touchscreen cognitive deficits, hyperexcitability and hyperactivity in males and females using two models of Cdkl5 deficiency. *Human molecular genetics*. 2022;31:3032-3050. doi: 10.1093/hmg/ddac091
192. Mottolese N, Uguagliati B, Tassinari M, Cerchier CB, Loi M, Candini G, Rimondini R, Medici G, Trazzi S, Ciani E. Voluntary Running Improves Behavioral and Structural Abnormalities in a Mouse Model of CDKL5 Deficiency Disorder. *Biomolecules*. 2023;13. doi: 10.3390/biom13091396
193. Downs J, Jacoby P, Specchio N, Cross H, Amin S, Bahi-Buisson N, Rajaraman R, Suter B, Devinsky O, Aimetti A, et al. Effects of ganaxolone on non-seizure outcomes in CDKL5 Deficiency Disorder: Double-blind placebo-controlled randomized trial. *Eur J Paediatr Neurol*. 2024;51:140-146. doi: 10.1016/j.ejpn.2024.06.005
194. Lau T, Miller T, Klein T, Benbadis SR, Vale FL. Temporal lobe surgery in medically refractory epilepsy: a comparison between populations based on MRI findings. *Seizure*. 2014;23:20-24. doi: 10.1016/j.seizure.2013.09.004

195. Tabibian F, Mehvari Habibabadi J, Maracy MR, Kahnouji H, Rahimi M, Rezaei M. Evaluation of Cognitive Impairment in Refractory Temporal Lobe Epilepsy Patients Concerning Structural Brain Lesions. *Basic Clin Neurosci*. 2023;14:385-395. doi: 10.32598/bcn.2022.3827.1
196. Frazzini V, Cousyn L, Navarro V. Semiology, EEG, and neuroimaging findings in temporal lobe epilepsies. *Handbook of clinical neurology*. 2022;187:489-518. doi: 10.1016/b978-0-12-823493-8.00021-3
197. Zhang C, Hu W, Wu Y, Li G, Yang C, Wu T. Altered Directed-Connectivity Network in Temporal Lobe Epilepsy: A MEG Study. *Sensors*. 2025;25. doi: 10.3390/s25051356
198. Ives-Deliperi V, Butler JT. Mechanisms of cognitive impairment in temporal lobe epilepsy: A systematic review of resting-state functional connectivity studies. *Epilepsy & Behavior*. 2021;115:107686. doi: <https://doi.org/10.1016/j.yebeh.2020.107686>
199. Ishizaki T, Maesawa S, Suzuki T, Hashida M, Ito Y, Yamamoto H, Tanei T, Natsume J, Hoshiyama M, Saito R. Frequency-specific network changes in mesial temporal lobe epilepsy: Analysis of chronic and transient dysfunctions in the temporo-amygdala-orbitofrontal network using magnetoencephalography. *Epilepsia open*. 2025;10:557-570. doi: 10.1002/epi4.70018
200. Alfiler L. ALLEN BRAIN ATLAS API. 2024.
201. Terzic B, Davatolhagh MF, Ho Y, Tang S, Liu YT, Xia Z, Cui Y, Fuccillo MV, Zhou Z. Temporal manipulation of Cdkl5 reveals essential postdevelopmental functions and reversible CDKL5 deficiency disorder-related deficits. *J Clin Invest*. 2021;131. doi: 10.1172/jci143655
202. Kind PC, Bird A. CDKL5 deficiency disorder: a pathophysiology of neural maintenance. *J Clin Invest*. 2021;131. doi: 10.1172/jci153606

Disclaimer/Publisher's Note: The statements, opinions and data contained in all publications are solely those of the individual author(s) and contributor(s) and not of MDPI and/or the editor(s). MDPI and/or the editor(s) disclaim responsibility for any injury to people or property resulting from any ideas, methods, instructions or products referred to in the content.